...ineering Center
...n–Madison

A REPORT
OF THE
SEVERE WEATHER PROGRAM
FOR THE PERIOD
1 SEPTEMBER 1992 TO 31 DECEMBER 1993

A REPORT from the

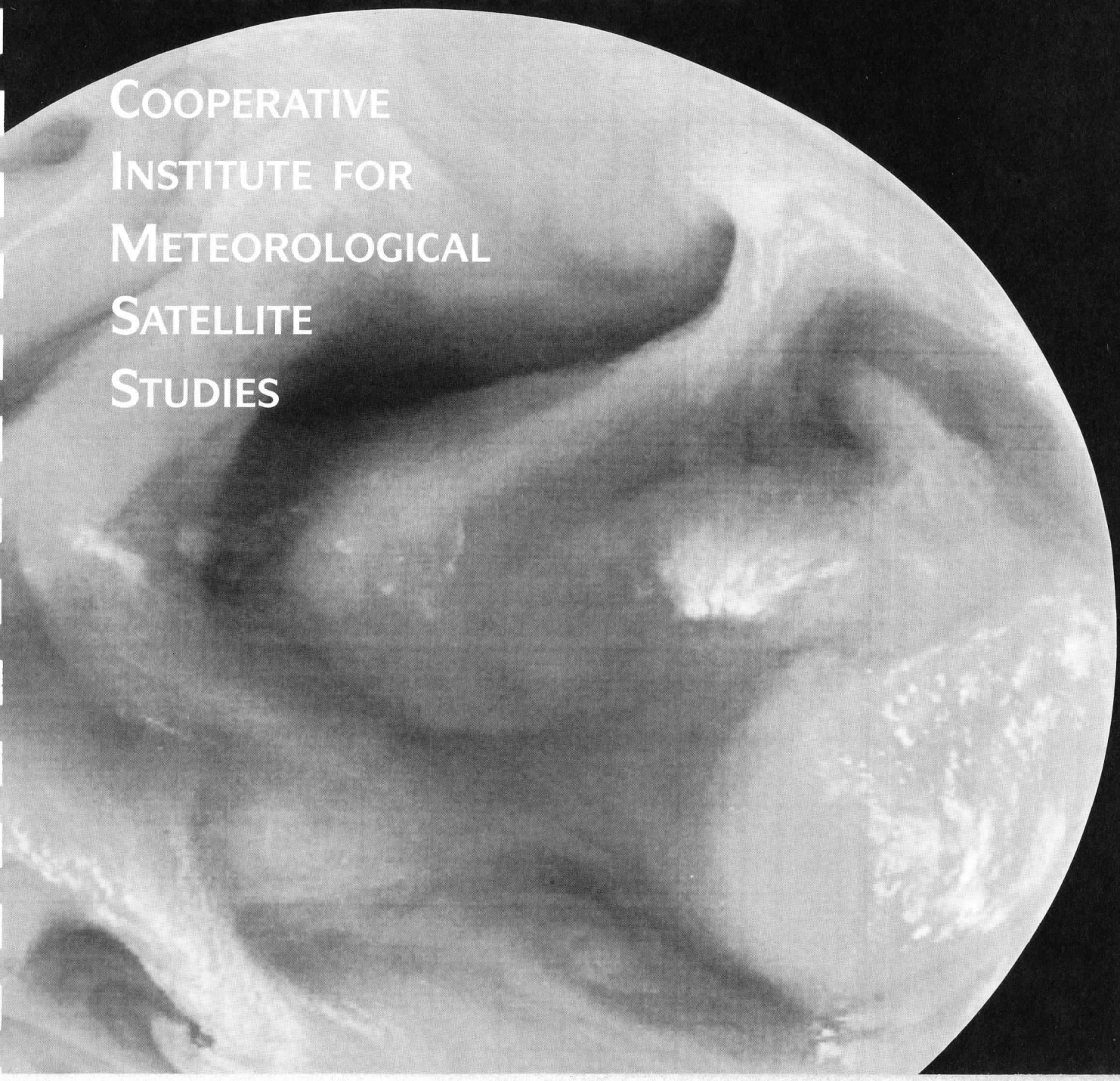

COOPERATIVE INSTITUTE FOR METEOROLOGICAL SATELLITE STUDIES

A REPORT OF THE SEVERE WEATHER PROGRAM FOR THE PERIOD 1 SEPTEMBER 1992 TO 31 DECEMBER 1993

Submitted by

Cooperative Institute for Meteorological Satellite Studies
Space Science and Engineering Center (SSEC)
at the University of Wisconsin-Madison
1225 West Dayton Street
Madison, Wisconsin 53706
(608) 263-7435

William L. Smith
Director, CIMSS
Principal Investigator

Anthony J. Schreiner
Associate Researcher
Program Manager

Christopher M. Hayden
Chief, SDAB
Principal Scientist

I. INTRODUCTION

This annual report describes the work done during the final year of a three year funding period. The period covered is from 1 September 1992 through 31 December 1993. The scope of this report is twofold: first, to give a brief summary of the various and diverse projects being funded during the contract period (RESULTS); second, to denote the personnel supported and equipment acquisition needed to accomplish the goals detailed in section II (PERSONNEL AND EQUIPMENT). Sections IV and V summarize and list references, respectively. The reference section includes all published papers and conference reports resulting from this research work plus the sited articles in the Results section.

The five main research areas covered in this report are:

- The use and development of the CIMSS Regional Assimilation System (CRAS) model at CIMSS. The CRAS has gone through extensive streamlining and improvements since it was first introduced to the modellers at the University of Wisconsin in 1982. Three articles discuss the development of this hybrid version of the Australian Numerical Research Centre regional model as an assimilation system for satellite products.
- Development of satellite-derived products using the VISSR Atmospheric Sounder (VAS). Three areas are examined. One describes a technique to obtain upper level atmospheric moisture by exploiting the water vapor bands aboard the VAS. A second details research in the use of atmospheric temperature/moisture retrievals during the Great Atlantic Low Experiment (GALE). The final area uses VAS-derived moisture information to better understand the three dimensional distribution of water vapor in the Gulf of Mexico.
- Techniques to improve the retrieval of surface parameters from remote sounders. Two studies examine the use of remotely sensed radiance information to define sea surface temperature (SST). One method using AVHRR data investigates a technique to eliminate contamination due to volcanic dust. A second method exploits the multi-banded HIS instrument in defining SST.
- Continued development of the High resolution Interferometer Sounder (HIS) and its performance in the Convection and Atmospheric Moisture EXperiment (CAMEX). A description of the CAMEX and the role the HIS played in this field experiment is discussed.
- The problem of obtaining cloud motion vectors in the polar region and the techniques for detecting them.. A comparison of a cluster fitting and cloud tracking technique for obtaining cloud motion vectors is examined over the Arctic. The benefits and drawbacks for each is discussed.

II. RESULTS

A. The CRAS Real-Time Forecast Systems and the Assimilation of VAS Precipitable Water. Contributed by Robert M. Aune.

A major goal of the Modeling Group at CIMSS has been achieved. Real-time numerical weather predictions, assimilating research data from weather satellites are being produced routinely using the CIMSS Regional Assimilation System (CRAS). Control and experimental forecasts are being compared to assess the impact of the remotely sensed data. Real-time assimilations using the CRAS have been produced twice daily since 1 February, 1992.

Two systems are currently running, real-time, on two IBM RISC 6000's: a fine-mesh (80 km) and a coarse-mesh (155 km). Recent updates to the real-time systems include: 1) vertical resolution of the fine-mesh forecast (80 km mesh) was updated from 20 to 24 levels to improve boundary layer accuracy; 2) the 12 hr forecast from the previous run is now used as the background to the analysis (instead of the NGM analysis from NMC); 3) an explicit cloud prediction scheme was added (Perkey, 1976); 4) surface temperature is now analyzed to improve boundary layer accuracy; 5) a snow cover analysis was added to improve high/low temperature predictions. Details of the forecast systems are presented in Table 1.

	Fine-mesh	Coarse-mesh
Type:	Semi-Implicit P.E. Non-hydrostatic	
Resolution; Horizontal (km):	80	155
Vertical levels (Sigma):	24	20
Grid size:	85x67	61x47
Time step (sec):	400	720
Forecast length (hours):	48	72
Output interval (hours):	3	6
Initial times (UTC):	00/12	00/12
Execution times (Local):	0200/1700	0230/1345
CPU time (min.):	235	120
Analysis guess:	CRAS 12 hr. Fcst	
Analysis input data:	RAOBS/AVHRR SST/SFC	
Verification data:	RAOB/SFC/SAT	
Parallel research forecast:	no	yes
Current applications:	UW Looper AMSU OSSE	VAS Assimilation Cloud Track Winds

Table 1. Current CRAS configurations. OSSE represents Observing System Simulation Experiment.

Since the coarse-mesh operation was implemented on February 1 a 97% completion rate has been achieved. All failures were a result of the nonreceipt of initial data.

In addition to the regular scheduled assimilations the system supports for on demand requirements. A hurricane forecast model (119x75, 90 km. resolution) is currently being used test the sensitivity of hurricane track predictions to water vapor winds from METEOSAT. Other forecasts are also produced to support case studies by CIMSS scientists and University students.

Since May 1993 precipitable water retrievals from the VISSR Atmospheric Sounder have been incorporated into the 155 km version of CRAS. The technique used to assimilate the data was designed to adjust the forecast moisture profiles to match the total precipitable water observed by VAS. Objective verification using 24 hour precipitation observations show that the VAS moisture data can have a positive impact on 24 hour precipitation forecasts in certain synoptic situations and in certain regions. Figure 1 shows total precipitable water differences, VAS minus NOVAS, valid 8 February, 1994 at 00 UTC. Figure 2 shows the 24 hour accumulative precipitation forecast with the VAS data valid 9

February, 1994, 00 UTC. The total precipitable water from VAS increased the 24 hour total precipitation totals over California and are in better agreement with the observed rain gauge network.

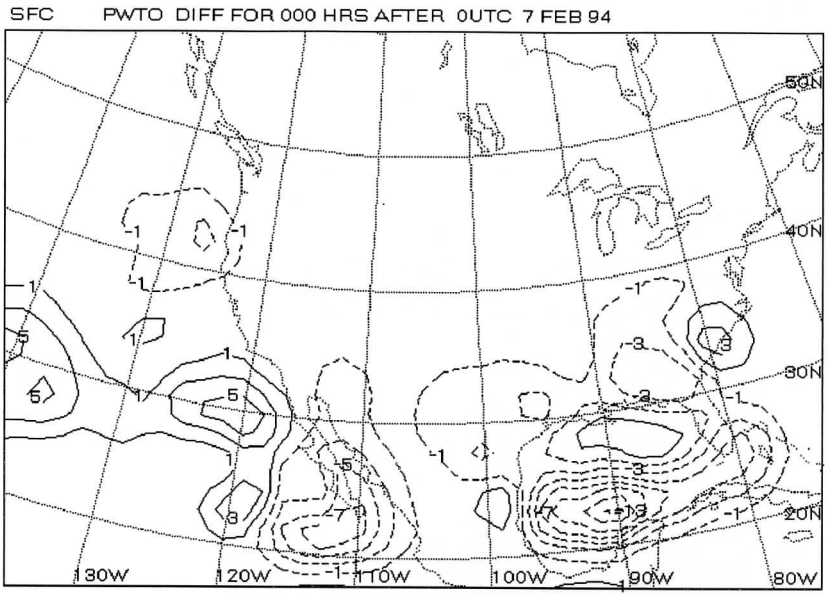

Figure 1. Total precipitable water differences. VAS minus NOVAS. Valid 8 February 1994 00 UTC.

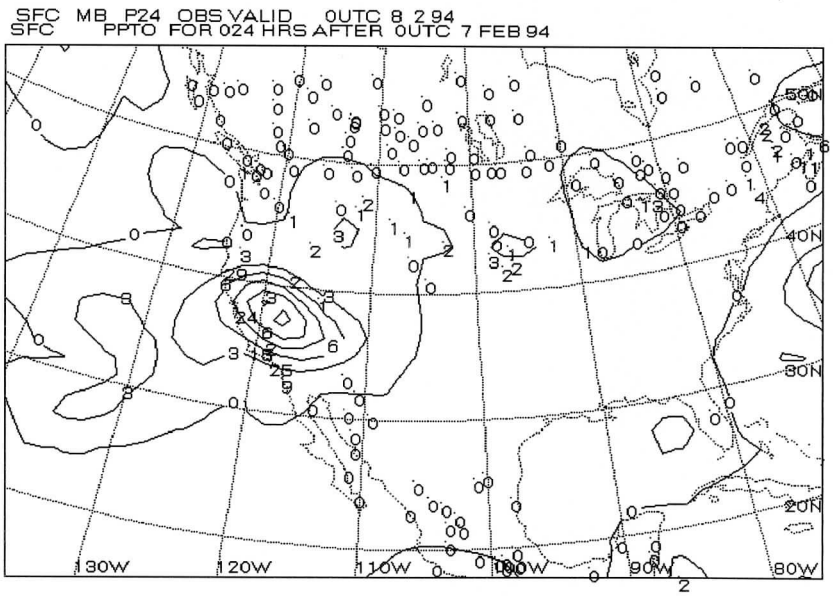

Figure 2. The twenty-four hour accumulative precipitation forecast with the VAS data valid 9 February 1994 00 UTC.

B. Short-Range Precipitation Forecasts Using Assimilation of Simulated HIRS-AMSU Water Vapor Profiles and Cloud Liquid Water. Contributed by Xiaohua Wu.

This work presents and examines some numerical techniques for the assimilation of satellite-observed water vapor and cloud liquid water into the CRAS in order to shorten the precipitation spin up time and improve short-range forecasts. A series of Observing System Simulation Experiments (OSSE's) were performed to (a) assess the probable impact of the upcoming NOAA KLM HIRS-AMSU data (temperature, moisture and total column cloud liquid water content data), and (b) test two key aspects of initialization procedures (cloud water initialization and diabatic initialization) making use of satellite observed moisture and cloud water data. The assimilation procedure diagnoses the existing cloud, improves the initial water vapor mixing ratio distribution, and uses diabatic initialization to produce significant divergent motions in the initial state.

Based on a satellite estimate of total column cloud liquid water and satellite (or rawinsonde) observed water vapor mixing ratio profiles, the initial cloud water distribution is specified through a diagnostic method. The initial humidity analysis is then updated by enhancing the relative humidity within the cloudy area. The latent heat release from the CRAS convective and large scale condensation with the enhanced moisture fields is incorporated into a vertical mode initialization (VMI) in an attempt to reduce the spin up time of the vertical circulation, and thus improve short range precipitation forecast.

Many previous studies have demonstrated that if diabatic heating rates are known, the normal mode initialization procedure can produce significant divergence in the initial state. It was our desire to see if the same procedures would apply with the VMI of the CRAS, and also to see if the results could be enhanced with satellite observations. An analysis of the dynamic balance induced by adiabatic and diabatic VMI affirmed that adiabatic initialization is unable to generate the initial divergent circulations which are diabatically driven by precipitation processes. With large scale diabatic heating rates, diabatic initialization can generate these circulations, which are consistent with the heating sources. A main feature to note is that diabatic initialization is effective only when a few of the higher vertical modes are initialized. For the CRAS, a vertical mode with the gravity wave phase speed equal to 40 m/s (corresponds to mode =3) must be initialized. Another important feature is that nonlinear normal mode initialization (or VMI type) balance conditions appear to be appropriate only for large gravity wave phase speeds (or large equivalent depths). The initialization of higher modes with smaller gravity wave phase speeds disturbs the quasi-geostrophic balance in the CRAS, and the subsequent forecasts are not realistically smooth. To guarantee the dynamic balance induced by diabatic VMI in the subsequent forecast, the 3-mode limit was employed in

the diabatic VMI for most satellite data assimilation experimental forecasts in this work. (This limit is equivalent to a 6 mode limit for the global climate model.)

The results from two synoptic case studies, corresponding to a warm front (case 1) and a cold front (case 2) precipitation system, respectively, are summarized in Figure 1 and Figure 2. Several experiments are compared to a control forecast which is the second twelve hours of a twenty-four hour forecast. Figure 1.a shows the accuracy of accumulated hourly precipitation rates (P_{total}) at the third hour of the forecast period compared to the control forecast (assumed as a "correct" forecast) for case 1. Figure 1.b summarizes the spin up time for each OSSE forecast when P_{total} reached 70% of that in the control forecast. The results indicate that diabatic initialization alone (NOSAT+DI) does not produce an accurate precipitation rate in the early stages of the forecast; the accuracy of P_{total} is only 42%, and the spinup is not improved from the eleven hours shown by the NOSAT+A1. Similarly, using adiabatic initialization with only satellite observed temperature (T) and water vapor mixing ratio (q) profiles NOCW+A1 failed to improve P_{total}, although this experiment shortened the spin up time from 11 hours to 6 hours. By applying satellite observed T and q profiles, specifying an initial cloud water distribution and improving the initial moisture distribution in cloudy areas, the forecast (SAT+AI) obtained significant improvement in P_{total}; an accuracy of 60% was obtained and the spin up time was decreased to 4 hours. However, with adiabatic initialization, the precipitation during the early stages of the forecast in some heavy rainfall regions was still deficient. Finally, adding the diabatic initialization, the forecasts (SAT+DI) produced rainfall patterns that fairly closely approximated those of the control experiment, especially in the large rain rate regions. In this case the accuracy of P_{total} reached 85% and the spin up time was decreased to 2.1 hours. The results from case 2 are summarized in Figure 2 which shows the accuracy of P_{total} at the third hour (a) and the eighth hour (b) of the forecast period. As indicated in Figure 1, the series of OSSE forecast runs for this cold front case shows the potential contribution of the satellite observed atmospheric temperature and moisture profiles to the short range precipitation forecast, especially at the eighth hour.

These experiments show convincingly that both vertical motion and moisture (cloud water) must be specified consistently to obtain reasonable precipitation in the early stages of a forecast. The assimilation of satellite observed cloud water together with the diabatic initialization is a crucial step to improve the precipitation spin up problem providing a capability to modify the initial water vapor distribution, to diagnose the existing clouds and to produce significant divergent circulations which are consistent with the latent heating sources. The improvement of initial water vapor distribution in cloudy areas plays an important role in shortening the precipitation spin up time. The experimental forecasts in this study also have

relevance to the application of cloud/precipitation observations from ground-based observational systems (e.g., NEXRAD).

To further improve the effectiveness of the present approach, it is necessary to develop a method based on other independent data sources (e.g., satellite precipitation or ground-based rainfall observations) to obtain more realistic 3 dimensional latent heating rates. Also, some continuous four dimensional data assimilation techniques (such as continuous nudging of satellite moisture and cloud data) are worth investigating.

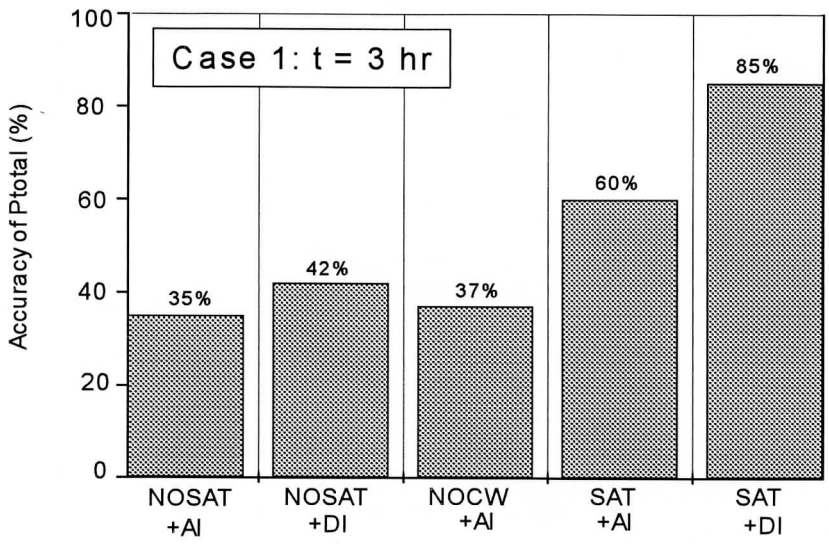

(a)

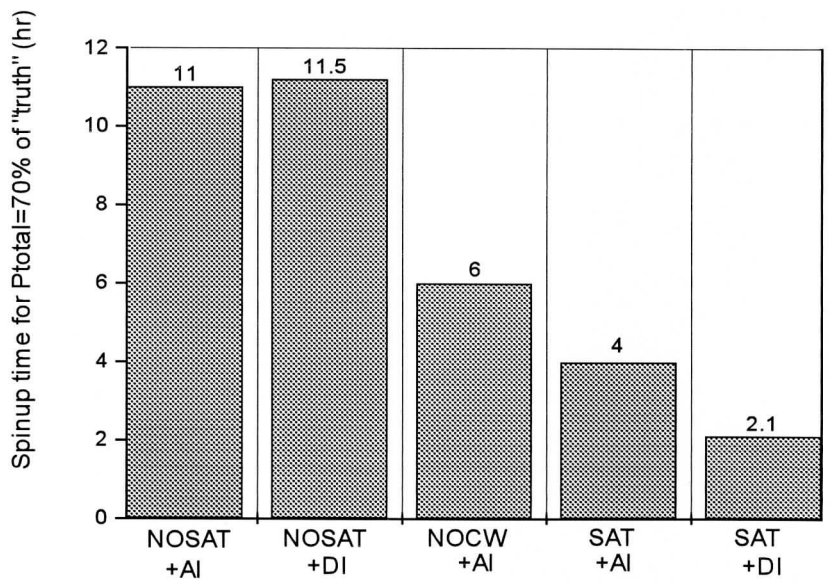

(b)

Fig. 1 (a) Accuracy of accumulated-hourly precipitation rates P_{total} at the third hour of the forecast period and (b) spin up time for $P_{total} = 70\%$ of that in control forecast for case 1.

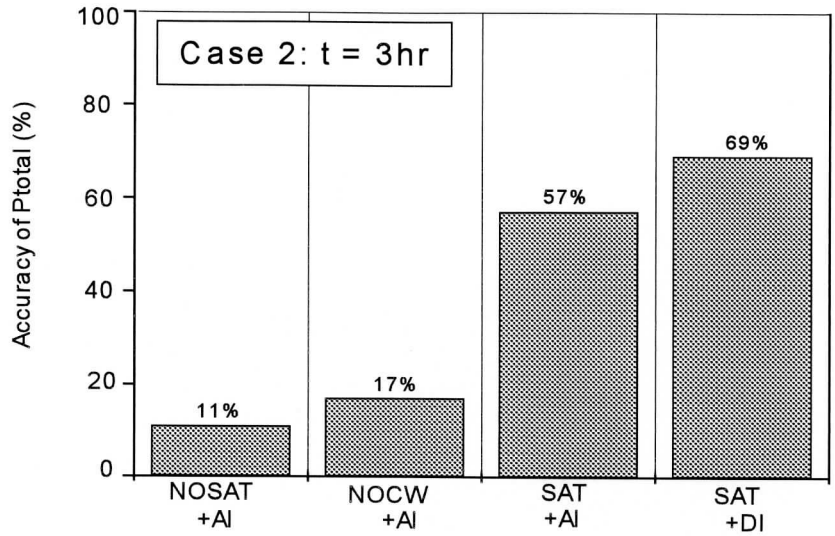

(a)

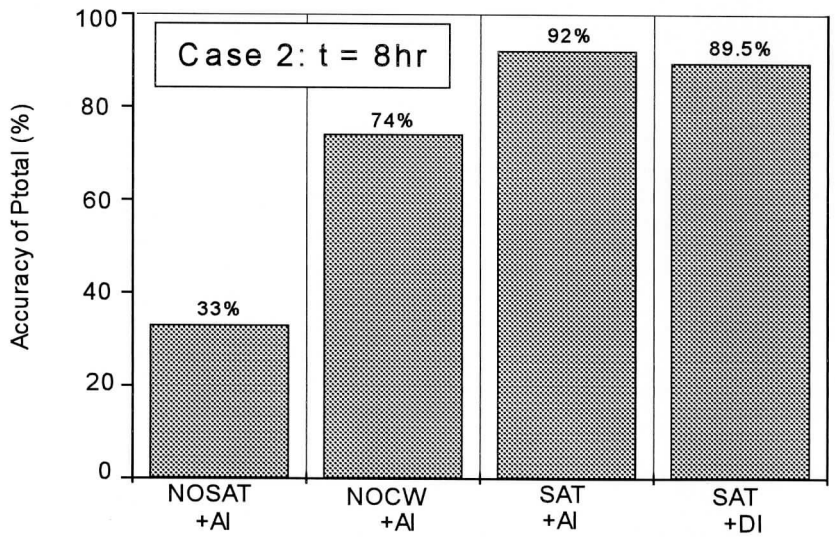

(b)

Fig. 2 Accuracy of accumulated-hourly precipitation rates P_{total} at the third hour (a) and the eighth hour (b) of the forecast period for case 2.

C. Improved Precipitation Forecasts Using Parameterized Feedbacks in a Hydrostatic Forecast Model. Contributed by William H. Raymond and Robert M. Aune.

Abstract

Excessive precipitation is a trait common to many hydrostatic forecast models. For quantitative accuracy, methods to control excessive diabatic activity must be used, but should not produce any negative impact on the model forecasts. Excessive precipitation is frequently controlled by applying a horizontal diffusion operator. While diffusion is helpful in some circumstances, negative consequences can occur if the horizontal smoothing is too heavy. In our study a parameterization of the non-hydrostatic mechanisms of precipitation drag and small-scale diabatically-induced mixing is used in the CRAS to curb excessive precipitation production. Non-hydrostatic processes are parameterized by a Newtonian damping procedure which is applied to the vertical acceleration in a manner similar to the quasi-hydrostatic approximation of Orlanski (1981). The Newtonian damping coefficient is proportional to the predicted liquid rain water. A number of precipitation events have shown that heavy precipitation production is greatly curtailed by the parameterization, while light precipitation episodes are not impacted.

The Initialization of Moisture in Numerical Forecast Models

Modelers lack a "balance" equation to assist in the initialization of the mixing ratio field. Nevertheless, some initialization is required to resolve differences between model predictions and observational measurements. This is especially critical in the vertical coordinate because of the rapid variations of mixing ratio with height. In our study, we impose a variational constraint to improve our initial moisture field by requiring that the distribution be consistent with the partial differential equation governing the mixing ratio.

Vertical motion either enhances or suppresses the vertical transport of moisture depending upon the sign of the vertical velocity ω (pressure coordinate). The importance of the vertical motion is reflected in the mixing ratio equation, which can be written as

$$L \equiv \frac{\partial q}{\partial t} + \omega \frac{\partial q}{\partial p} + R = 0 \qquad [1]$$

Here t represents time, q the mixing ratio and R symbolically represents the remaining residual horizontal advection, forcing and damping terms.

The optimal solution of (1) that minimizes differences between model calculations and observations requires the minimization of the functional

$$J = \int \left[\alpha^{*}(q - q^{*})^2 + \alpha^{+}(q - q^{+})^2 + \beta^{*}(R - R^{*})^2 + \beta^{+}(R - R^{+})^2 + \lambda L \right] dp \qquad [2]$$

where α and β are weighting factors and λ is the Lagrangian multiplier. Here * denotes model calculation while + superscripts denote initial analysis.

The optimal mixing ratio is obtained using the Euler equation of classical variational calculus, yielding

$$q = \frac{\left[\left(\alpha^{*} q^{*} + \alpha^{+} q^{+} \right) \dfrac{\partial(\omega^{*}\lambda)}{\partial p} \right]}{\alpha^{*} + \alpha^{+}}, \qquad [3]$$

while the Lagrangian multiplier λ satisfies

$$\frac{\partial^2 (\omega^{*}\lambda)}{\partial p^2} - \left(\frac{\alpha}{\beta} \right) A(\omega^{*}\lambda) = \alpha \left[\left(\frac{\partial q^{+}}{\partial p} - \frac{\partial q^{*}}{\partial p} \right) + \frac{(R^{+} - R^{*})}{2\omega^{*}} \right] \qquad [4]$$

Here $A = 1/\omega^{*2}$ and $\beta > 0$ can be adjusted to improve the minimization. In (4), the right hand side or forcing term contains differences in the vertical gradient and residual between model forecasted and measured mixing ratio quantities.

The types of adjustment made using (3) and (4) to simulate profiles of forecasted and measured mixing ratios are shown in Figure 1. In these calculations $\alpha^{*} = \alpha^{+} = 1$. The contribution from the Lagrangian multiplier is small, but sensitive to the type of boundary conditions or constraints used to solve (4).

Figure 1

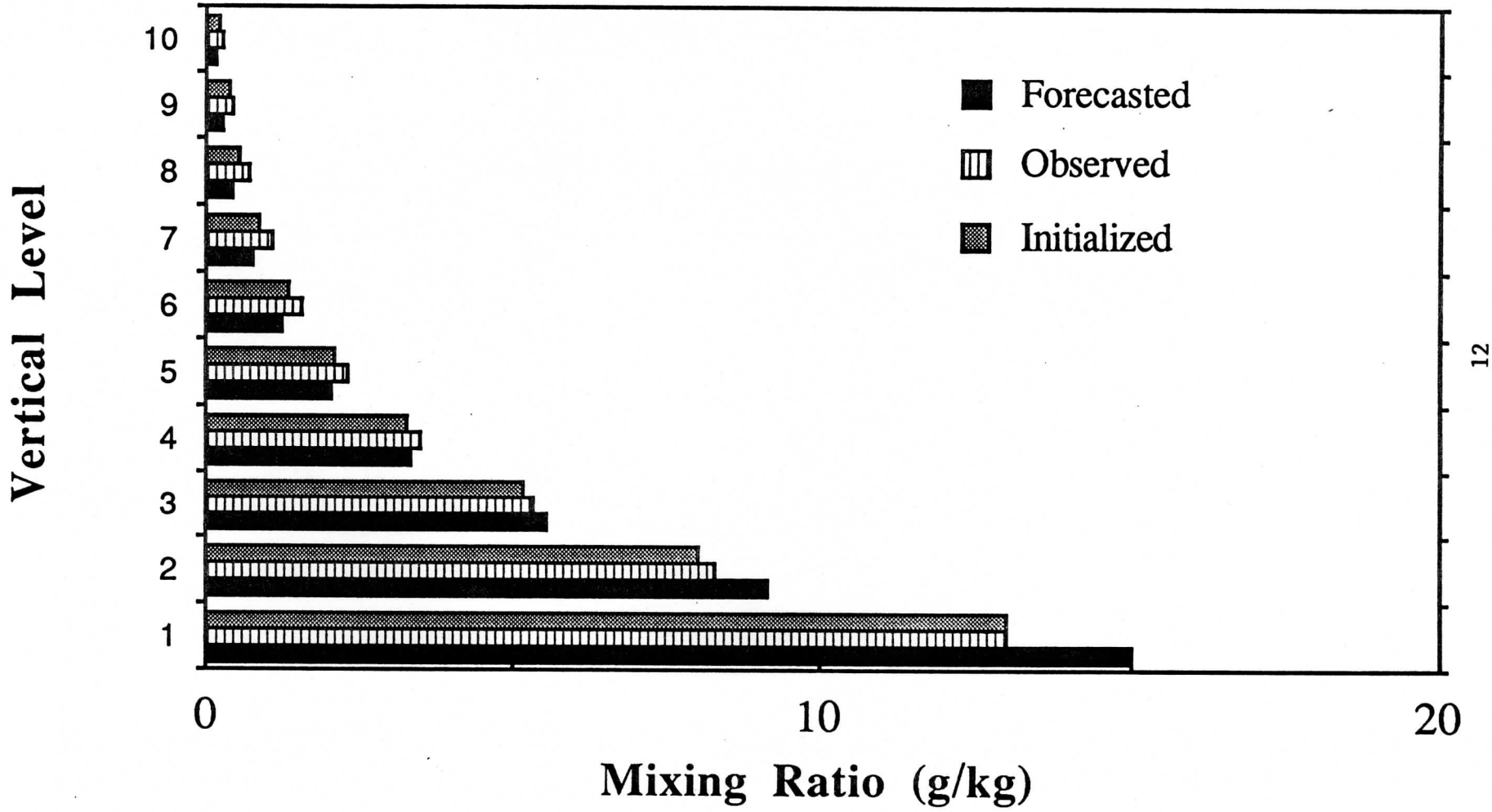
Vertical Level
10
9
8
7
6
5
4
3
2
1
Forecasted
Observed
Initialized
0
10
20
Mixing Ratio (g/kg)
12

D. Development of an Upper Tropospheric Relative Humidity (UTH) product for Geostationary Satellites with measurements in the 11 micrometer window and the 6.7 micrometer water vapor bands. Contributed by Christopher M. Hayden and Xiangqian Wu.

INTRODUCTION

The concept of inferring relative humidity from satellite measurements in the infrared windows and 6.7 micrometer water vapor band originated before there were any meteorological satellites (Moller, 1961). The first attempts at real data analysis were accomplished with TIROS IV data by Rasche and Bandeen (1967). The METEOSAT Exploitation Project of the European Space Operations Centre provided the first operational product from METEOSAT-3 in 1986. Currently, a grid product of Upper Tropospheric Humidity (UTH) is provided twice daily by the ESOC, and this is used by the European Centre for Medium Range Forecasting as part of their operational data base.

In addition to the potential utility of UTH in the initialization of numerical models, a second role relates to the study of climate and climate change. It is well recognized that minute quantities of water vapor in the upper atmosphere play a crucial role in regulating the earth's radiation balance (Starr and Melfi, 1991). A capability of routinely observing a quantitative UTH has obvious consequences to climate monitoring. This subject is currently under vigorous investigation (e.g. Wu et al., 1993; Soden and Bretherton, 1993). In most climatological applications, however, investigators have concentrated on the raw measurement, seeking trends in radiance space rather than in the more familiar meteorological realm of specific or relative humidity. Soden and Bretherton (loc. cit.) have specified an algorithm for the determination of relative humidity (over the layer 200 to 500 hPa), and have validated this by comparing their retrievals to vertically averaged relative humidity from rawinsonde profiles. In this they have achieved high accuracy with a correlation of 0.94 and an RMS of 6.2% using a sample of CLASS soundings taken during the FIRE Cirrus-II Intensive Observation Periods (Soden et al., 1994). A shortcoming of this study is that the radiances used in the algorithm are synthesized from the same rawinsondes rather than being real measurements. As will be discussed below, our skill in synthesizing the water vapor radiances is questionable.

In the current work we have pursued several objectives. The principal one has been to define a system for operational processing of UTH from GOES data. Initially this is to be modeled on the ESOC product (Schmetz and Turpeinen, 1988), but it will be extended as explained in the next section. A second objective is to introduce the radiative transfer models developed at the Cooperative Institute for Meteorological Satellite Studies (CIMSS) and compare the product with the ESOC results. A third objective is to evaluate the accuracy of

the product in the manner of (Soden et al., 1994), but with real satellite measurements. Finally, we wish to consider the representativeness of the UTH with respect to application in numerical weather forecast models.

PROCESSING SYSTEM

The ESOC method for deriving UTH uses a temperature/moisture profile from a numerical forecast model at the location of a 32x32 pixel (each pixel has 5 km spatial resolution) processing element, and the cloud cleared 6.3 METEOSAT radiance. Between 600 and 300 hPa the moisture profile is replaced with 6 values of relative humidity (.01, .03, .07, .16, .40, and .99). Each of the six profiles is converted, via the forward radiative transfer equation, to an estimated radiance. The observed radiance is then used to interpolate within the calculated radiances to obtain the UTH estimate. (The relative humidity intervals were apparently chosen to allow linear interpolation of radiance, which varies very non-linearly with moisture. Our research has shown, however, that this does not work well.)

For the CIMSS system we first duplicated the METEOSAT radiative transfer and UTH product with some sample profiles provided by ESOC. For general application, however, we are using full resolution pixels (5 km for METEOSAT, but 14 km for GOES-7). The purpose is to create an image, rather than a grid, of relative humidity after the fashion of Derived Product Imagery which is used at NESDIS for operational products of precipitable water and lifted index derived from the VAS (Hayden and Schmit, 1989). No cloud clearing is attempted. Where cloud is present, the radiance temperature is low and high values of relative humidity are inevitable. In the imaged product we define any retrieval $> 90\%$ as cloud. This value was selected by visual examination of the UTH image compared with images of the METEOSAT water vapor and infrared window measurements. An example of METEOSAT-3 window, water vapor radiance, and the GOES-7 water vapor radiance (all mapped into the same projection) is shown in Figure 1. The UTH product produced from the lower two panels of Figure 1 is shown in Figure 2. Qualitatively, the derived image is reasonable, warm (dark) areas in the water vapor image show low UTH (the signal is not attenuated by moisture in the upper atmosphere), and values of UTH increase around the edges of higher cloud which affect the 6.3 channel measurement.

Figure 1

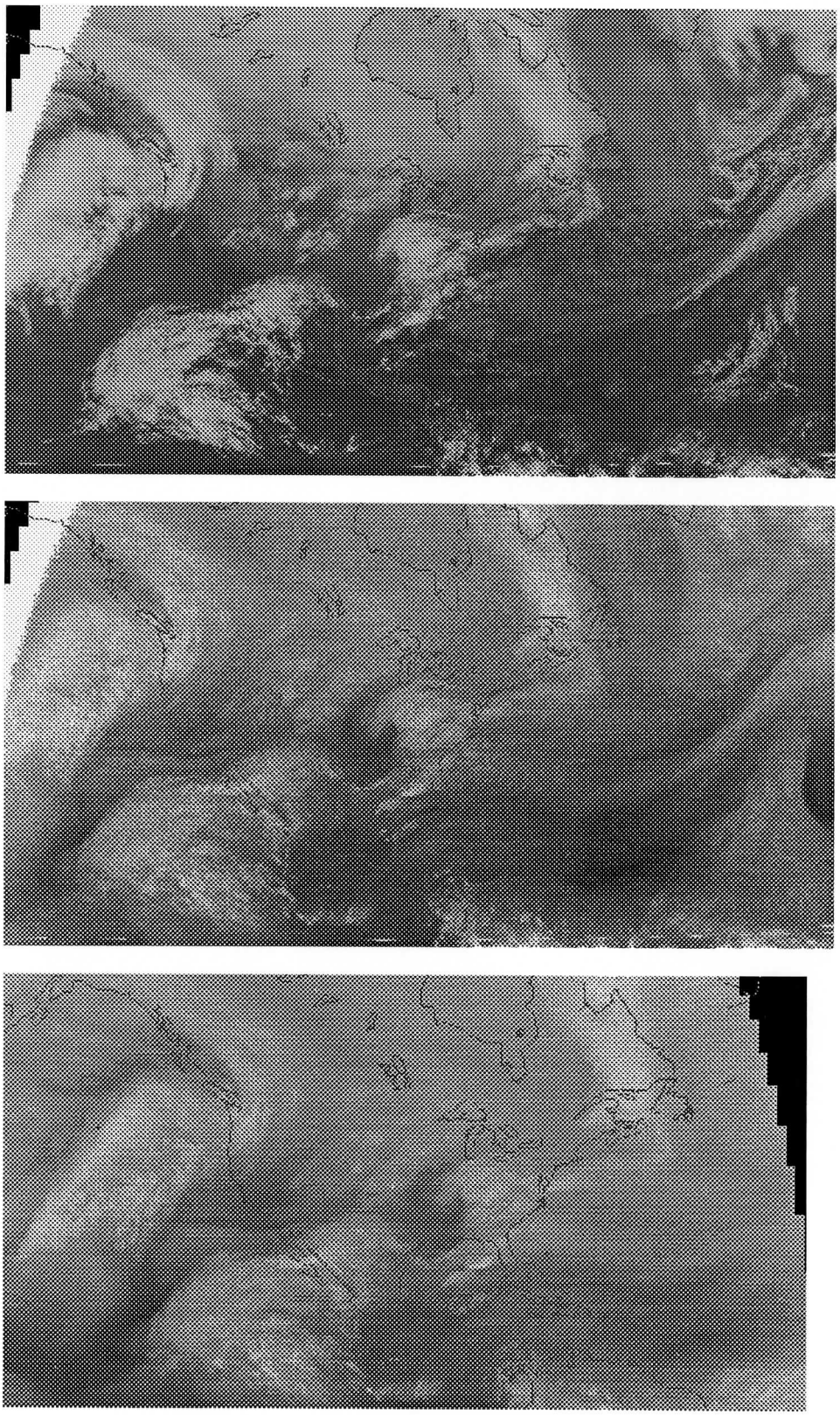

Figure 1. METEOSAT-3 infrared window (top) and water-vapor, 6.3 micrometer (middle) and GOES-7 water vapor, 6.7 micrometer (bottom images for January 11, 1994. Images have been remapped to common projection

RADIATIVE TRANSFER EXTENSION

Partly for the purpose of integrating the UTH processing into other operational GOES processing and partly to investigate the sensitivity of the algorithm to the radiative transfer modeling, we are in the process of adapting the CIMSS radiative transfer models to the UTH processing system. These models are based on recent line-by-line calculations and use a fast algorithm described by Eyre (1991). Models have been adapted for the polar orbiting TOVS satellites and also the GOES and METEOSAT. At present the implementation of the METEOSAT model to the UTH system is pending, but the implementation of the GOES for GOES-7 processing is complete. Since there is overlap between the METEOSAT-3, currently at 75W and GOES-7, currently at 112W, we can compare the UTH product derived with the ESOC transmittance model and METEOSAT data with that using the CIMSS transmittance model and GOES-7 data. The comparison is shown in Figure 2. (Note that the METEOSAT image has been remapped to the GOES-7 projection to facilitate comparison.) The same temperature/moisture forecasts from the NMC aviation model were used to process both data sets.

To begin on a positive note, the better horizontal resolution and lower noise of the METEOSAT measurement produce a more esthetic image, though this is not obvious in the figure shown. What is an obvious, and troubling feature of the comparison of Figure 2 is that a very large bias difference exists between the UTH estimates. The GOES product is much more moist. Values of relative humidity are approximately one color shade higher. We do not at this point have any ground truth to judge absolute accuracy, but it is virtually certain that these differences are caused by the different instrumentation; the METEOSAT channel is a broader band and "sees" deeper into the atmosphere. One feature of the GOES which seems more reasonable is that the values transition smoothly from high relative humidity into cloud. The METEOSAT image has little high humidity except within the cloud. On the other hand, the cloud indicated in the GOES product appears less accurate than in the METEOSAT. Note especially along the east coast of North America. Of course the somewhat arbitrary thresholding of cloud at relative humidity greater than 90% would have this effect with the moister GOES estimates.

Although we do not have the CIMSS METEOSAT transmittance model fully integrated into the UTH processing, we are able to produce METEOSAT radiance temperatures for individual temperature/moisture profiles, and this has allowed us to compare the performance of the CIMSS vs. the ESOC transmittance modeling. Seventy-five points were chosen from

the data shown in Figure 1 where the 11 micrometer window was at least as warm as the surface air temperature indicated in the NMC forecast. The scatter plot of the forward calculation using the GOES model or the ESOC model vs. the observation is shown in the top (bottom) panel of Figure 3. It appears that both models are biased relative to the observation, with the CIMSS model more severely, 5.9 K vs. 2.3 K too cold. This certainly accounts for why the GOES UTH is the wetter, but does not conform with the qualitative evaluation suggested in the comparison of the two UTH images above, namely that the METEOSAT product is too dry. A part of the bias may be attributable to error in the forecast, but our experience has been that the NMC aviation forecast is not notably biased with regard to forward calculations, at least for samples gathered in the mid latitude northern hemisphere. In support of this Figure 4 represents a scatter plot of GOES-7 forward calculations vs. observations at 6.7 micrometers collected during December, 1993 over the region 23-53N; 40-160W. While there is clearly disagreement between the forecast determined value and the measurement, the bias is small. Possibly the day represented by Figure 3 is simply atypical.

A second feature to note in Figure 3 is that the ESOC model gives less variance than is observed over the sample (the regression line is less than 45 degrees). In fairness, the regression line overemphasizes this deficiency, but the deficiency exists. It cannot be attributed to forecast error, since an equivalent feature is not seen with the CIMSS model. Also, the CIMSS GOES model shows only a slight variance attenuation (again in the northern hemisphere) in Figure 4. The deficiency can be anticipated to translate into a slightly unrealistic variance in the ESOC UTH.

SENSITIVITY EXPERIMENTS

The same sample of CLASS soundings gathered by Soden et al., (1994) has been used to derive UTH with the ESOC algorithm as applied to GOES-7 data. Two GOES transmittance models have been used, the newest model referenced above and the previous operational model. In this experiment cloud clearing was attempted by gathering all GOES observations within 1 degree latitude of each CLASS sounding and discarding any observation where the 11 micrometer infrared window radiance temperature was colder than the 700 hPa temperature of the CLASS sounding. Survivors were averaged to give the observed radiance temperature used to interpolate between the UTH estimates. Results for the two models are given in Figure 5. (The difference in sample sizes in Figure 5 is caused by removing any calculated relative humidity which exceeds 95%.) They are not impressive, certainly far less so than the results given by Soden et al., (1994) with an alternative algorithm. There is some improvement indicated with the upgraded transmittance model, but scatter and bias remain high, the latter much more than can be accounted for by a perceived dry bias in the CLASS.

The extreme difference between this result and that of Soden et al., (1994) is not known, and it is perplexing. Certainly the use of real rather than synthesized measurements contributes. Possibly also related is the choice of the layer bounding the UTH (300-600 hPa vs. 200-500 hPa).

REPRESENTATIVENESS

A final topic of interest, following up on the previous section, is to consider how representative the UTH is of the layer over which it is defined. To this end, UTH was calculated from full VAS retrievals of temperature and moisture for one of the FIRE-Cirrus II cases (December 7, 1991). Results are presented in Figure 6. Visually the UTH calculated from retrievals between 620 and 300 hPa corresponds well with the GOES imagery of the 6.7 micrometer measurement; much better than does the UTH calculated from the forecast. However, it is difficult to see close correlation between the UTH and the relative humidities retrieved at individual levels, as shown in Figure 7. And even though one can put little faith in the accuracy of the VAS retrievals of moisture at individual levels, this result certainly suggests that the definition of the layer over which UTH is defined is critical. And this is not surprising, since the contribution function for the 6.7 micrometer channels will move up and down over a range of about 200 hPa according to the ambient moisture. Referring again to the bias of Figure 2, the representativeness is clearly questionable.

Figure 2. Derived UTH for Meteosat (top) and GOES (bottom) for the case shown in Figure 1.

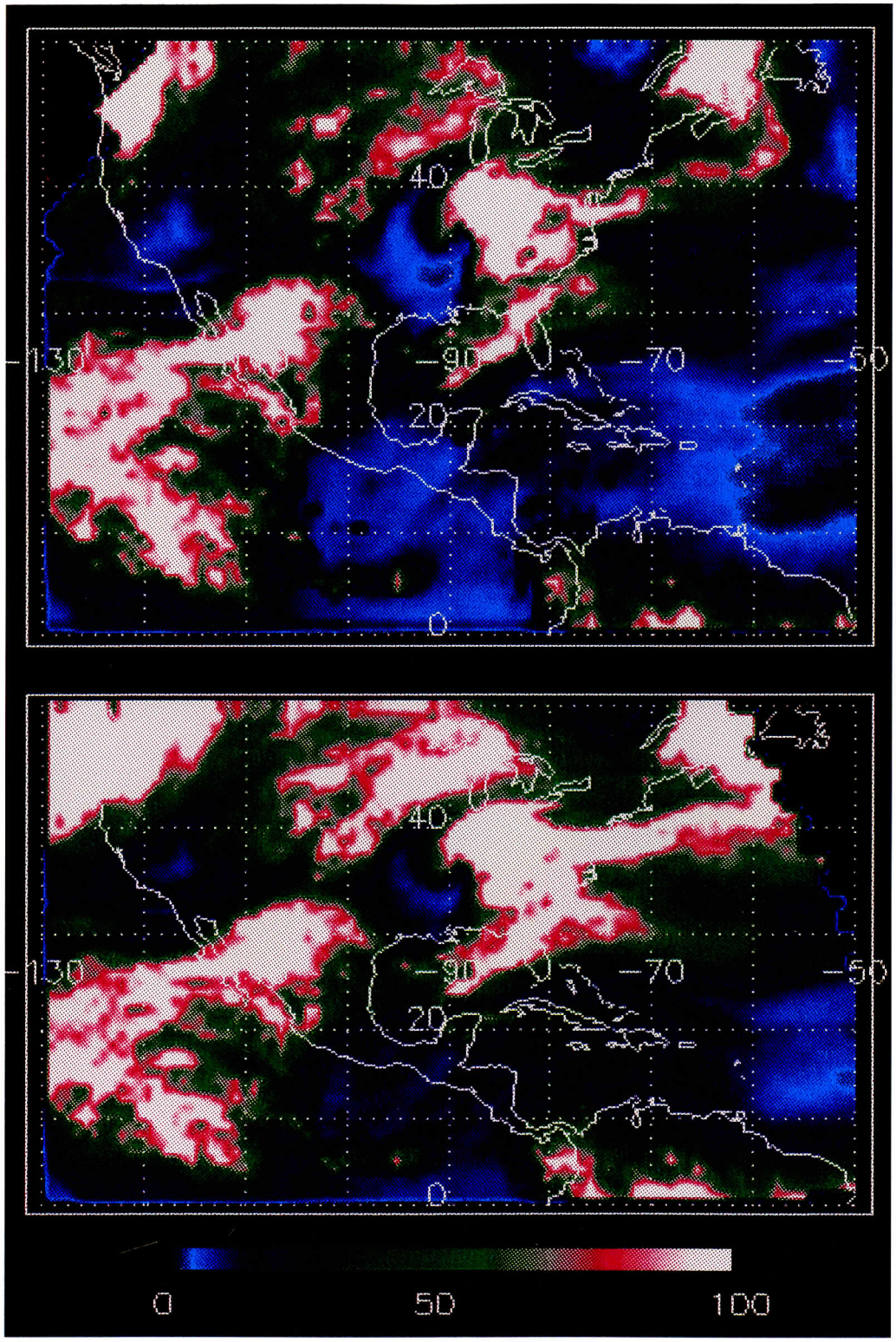

Figure 3a

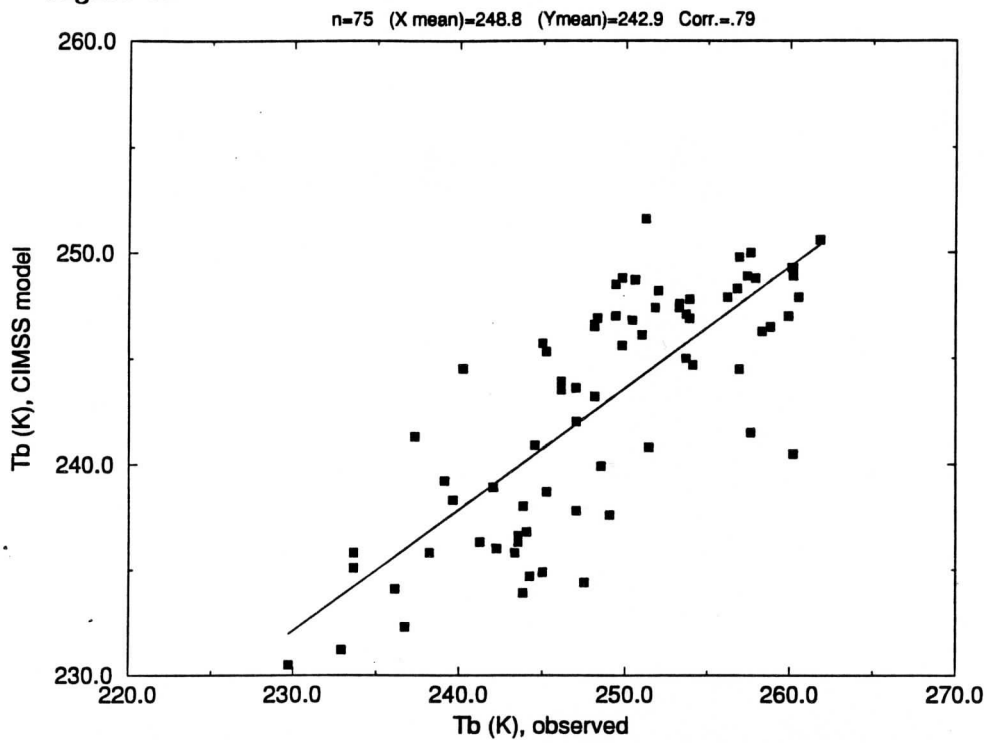

Figure 3b

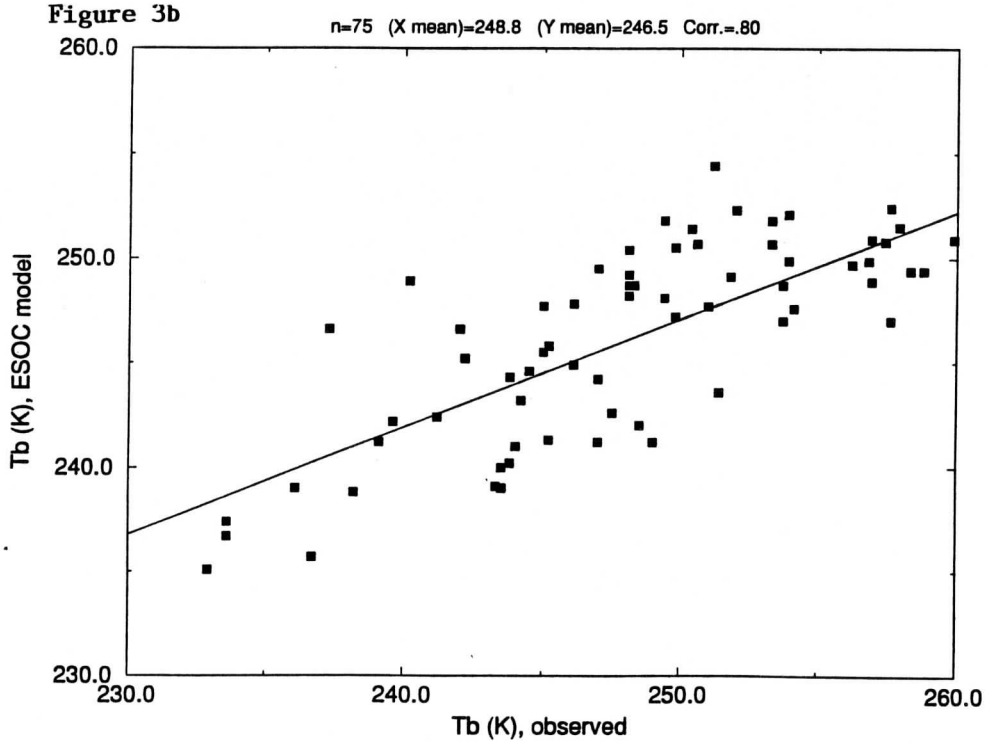

Figure 3. Scatter diagrams of observed vs. calculated radiance temperatures for Meteosat - 3 6.3 micrometer channel. a) CIMSS radiative transfer model. b) ESOC radiative transfer model. Calculations are based on NMC aviation forecast.

Figure 4

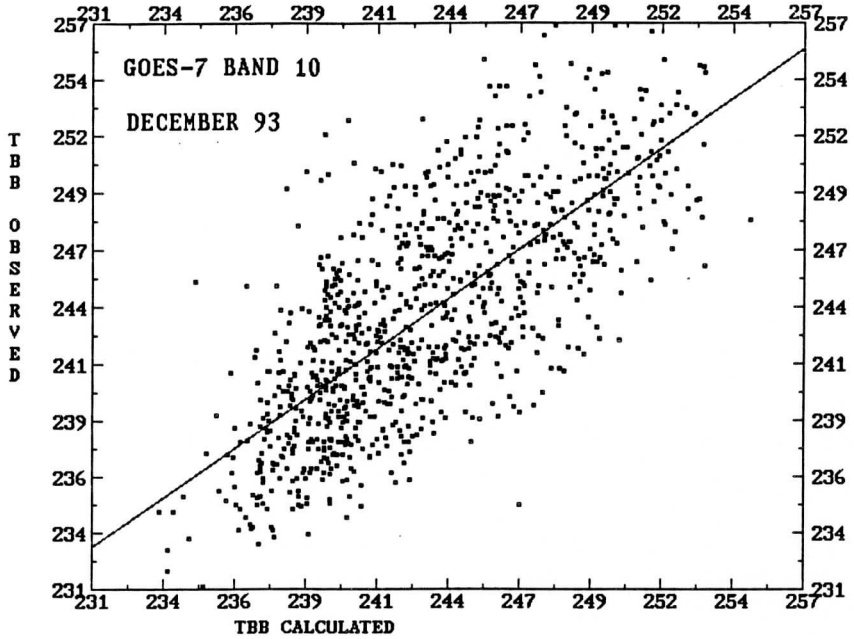

Figure 4. Scatter diagram of observed vs. calculated radiance temperatures for GOES - 7 6.7 micrometer channel. Values taken from operational processing, December 1993. Calculations are based on NMC aviation forecast.

Figure 5

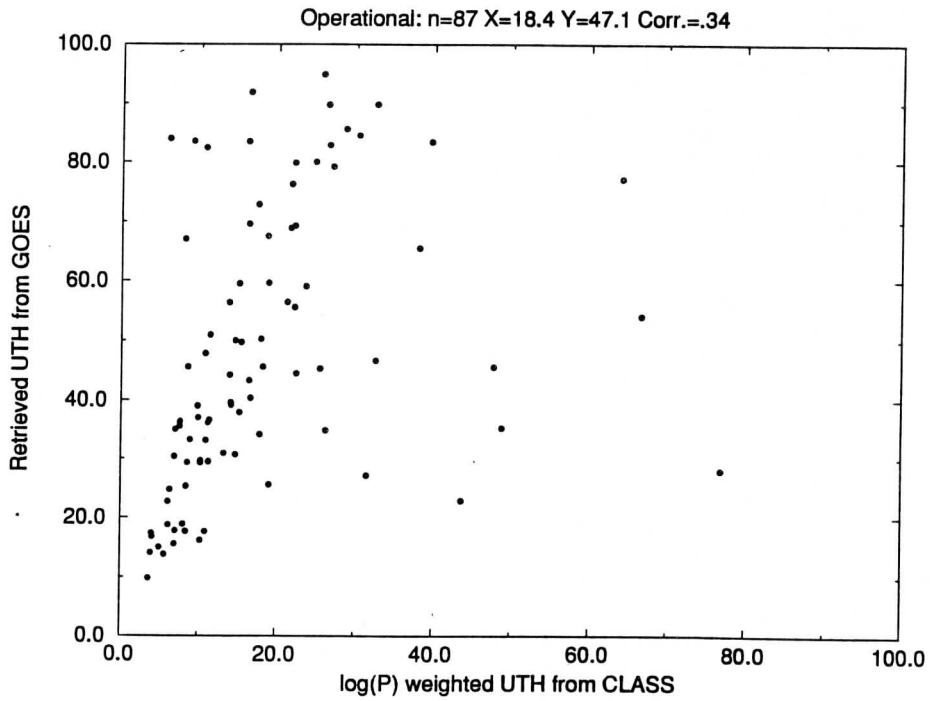

Figure 5. Comparison of UTH derived from operational and "upgraded" CIMSS transmittance models. Calculations are made from CLASS data obtained during FIRE experimet for collocated GOES - 7 measurements. a) operational model. b) upgraded model.

Figure 6

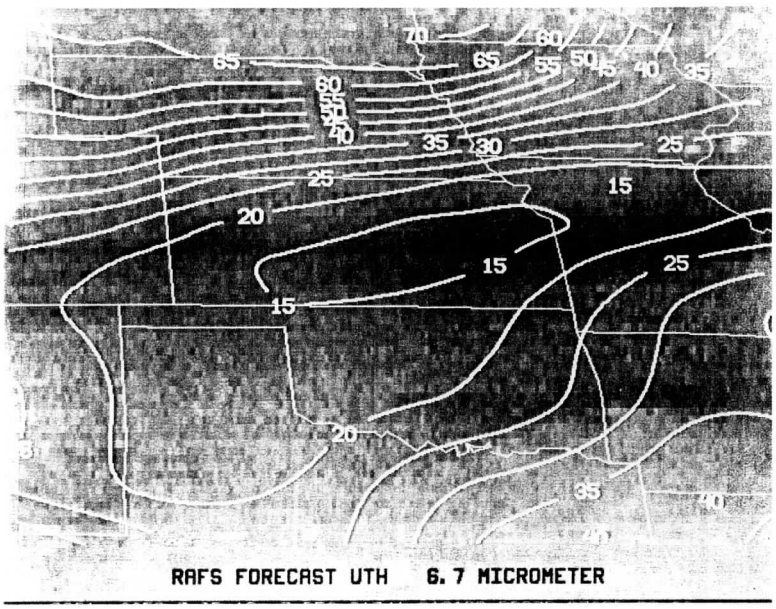

Figure 6. UTH computed from GOES - 7 VAS retrieval (left) and from the NMC Regional Forecast. Contours are over the GOES - 7 6.7 micrometer image.

Figure 7

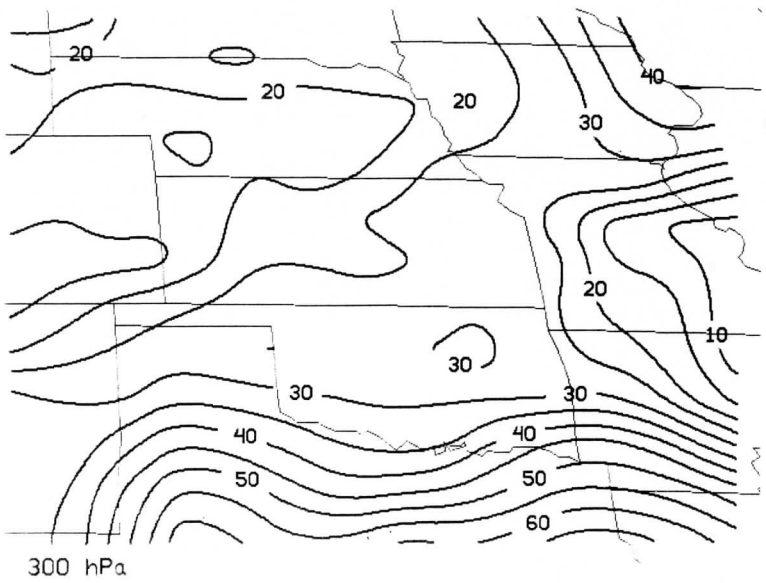

Figure 7. Four levels of retrieved relative humidity from the VAS retrievals. Levels correspond to depth averaged to provide UTH.

E. VAS-Derived Products. Contributed by Gary S. Wade.

VAS Retrieval Generation for GALE IOP-2.

Dr. Frank Ruggiero, originally at North Carolina State University (Raleigh, NC) and now at the Naval Research Laboratory (Washington, DC), requested VAS Dwell Sounding retrievals made during the second GALE Intensive Observation Period (IOP) which occurred from 24 to 28 January 1986. Ruggiero wished to acquire the VAS data for use in an assimilation experiment. He desired to use both the full retrieved profiles as well as actual radiance values. Although files existed with such profiles of temperature and moisture derived from the VAS dwell sounding observations at the time of the experiment, much has changed in the retrieval software over the last seven years. Only by reprocessing the retrievals with the current software would there be sufficient confidence in the product to support its dissemination.

Twenty three "pairs" of VAS Dwell Sounding radiance areas were available from GALE IOP-2, nominally at 1100, 1430, 1730, 2030, and 2300 UTC each day. Due to rapid scan operations or other difficulties, all times were not available on all days. Surface analyses (from surface, ship, and buoy reports) and first-guess fields (from global NMC model data) were created for each retrieval data set. A representative set of bias coefficients was generated for the period using cloud-cleared radiances and appropriate first-guess fields.

An average of 494 retrievals were produced for each pair of dwell sounds, covering the eastern half of the U.S. Due to varying cloud cover, the range was large, from a low of only 302 to a high of 721. The original files contained slightly more per time (an average of 514), with less variation (range of 358 to 631), for approximately the same areal coverage. No extensive statistical comparison was done with the new retrievals; qualitative assessment showed general agreement with the previous results. One significant improvement appeared to be the current cloud filtering routine. The extensive cloudiness during many of the time periods produced large regions void of retrievals.

Ruggiero acquired the data through the McIDAS workstation at NCSU-Raleigh during the fall of 1993. The McIDAS MD-files contained both the atmospheric profiles as well as the filtered and averaged radiance values for each profile (covering a 5x5 FOV box). An assessment of the satellite profiles is expected after Ruggiero has run his assimilation experiments.

Total Precipitable Water Estimates from VAS.

From previous experience in experiments such as GUFMEX (1988) and SWAMP (1990), CIMSS has maintained a strong interest in moisture observations from satellites. VAS-

MSI derived moisture products, such as the total precipitable water vapor (TPWV), have not always consistently presented positive information over the data-rich US mainland, such as during STORM-FEST (1992). However, satellites continue to provide useful information over oceanic and other regions void of conventional measurements (e.g. Figure 2a above). CIMSS has maintained a considerable effort in monitoring and assessing the CIMSS developed VAS-MSI products routinely produced on the NESDIS MIDAS computer in Washington. This is done with a particular emphasis on the coastal regions affecting the U.S.

TPWV data are also now readily available from the Special Sensor Microwave/Imager (SSM/I) onboard the polar orbiting DMSP satellites. The microwave products are obtained from regression relationships with rawinsonde profiles; the VAS TPWV data are obtained by radiative transfer determinations utilizing NMC forecast fields and the observed infrared radiances. The statistical SSM/I estimates are thus totally independent of the physically deduced VAS TPWV values. Combination of these complementary data sets (frequently available VAS data hindered by cloudiness versus rather limited but cloud oblivious coverage by the SSM/I) can provide for the most complete depiction of moisture fields surrounding and impacting the US mainland. With GOES-I, such composite analyses with available microwave data should continue.

Figure 1. VAS Dwell Sounding retrieval coverage at 1730 UTC on 23-28 January 1986 during GALE IOP-2 over the US East Coast. Values plotted are total precipitable water vapor (in mm).

Figure 2. Total precipitable water vapor product imagery for 26-27 January 1994 for: 1200 UTC from SSM/I; 1200, 1600, 2000, and 0000 UTC from VAS-MSI data; and 0000 UTC from SSM/I. Panels a and b are both valid for 1200 UTC; panels e and f, for 0000 UTC; and panels b-e, for each four hour from 1200 through 0000 UTC. The agreement between the VAS and SSM/I is very good at 0000 UTC; however, at 1200 UTC, the VAS appears too dry in the southwest Gulf of Mexico. Reasonable continuity is evident in the entire VAS four-hourly sequence.

Figure 1

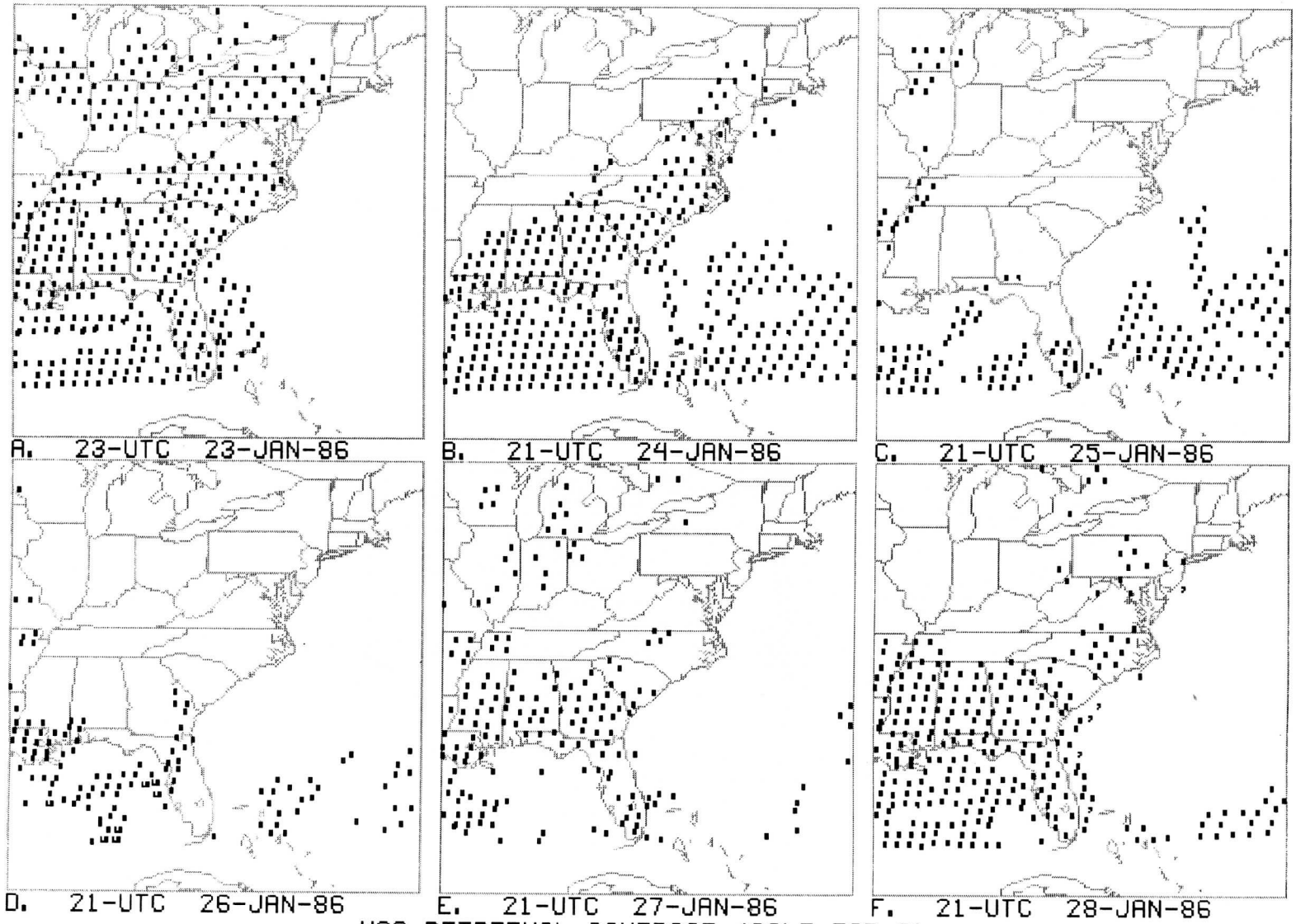
A. 23-UTC 23-JAN-86
B. 21-UTC 24-JAN-86
C. 21-UTC 25-JAN-86
D. 21-UTC 26-JAN-86
E. 21-UTC 27-JAN-86
F. 21-UTC 28-JAN-86
VAS RETRIEVAL COVERAGE (GALE IOP-2)

Figure 2

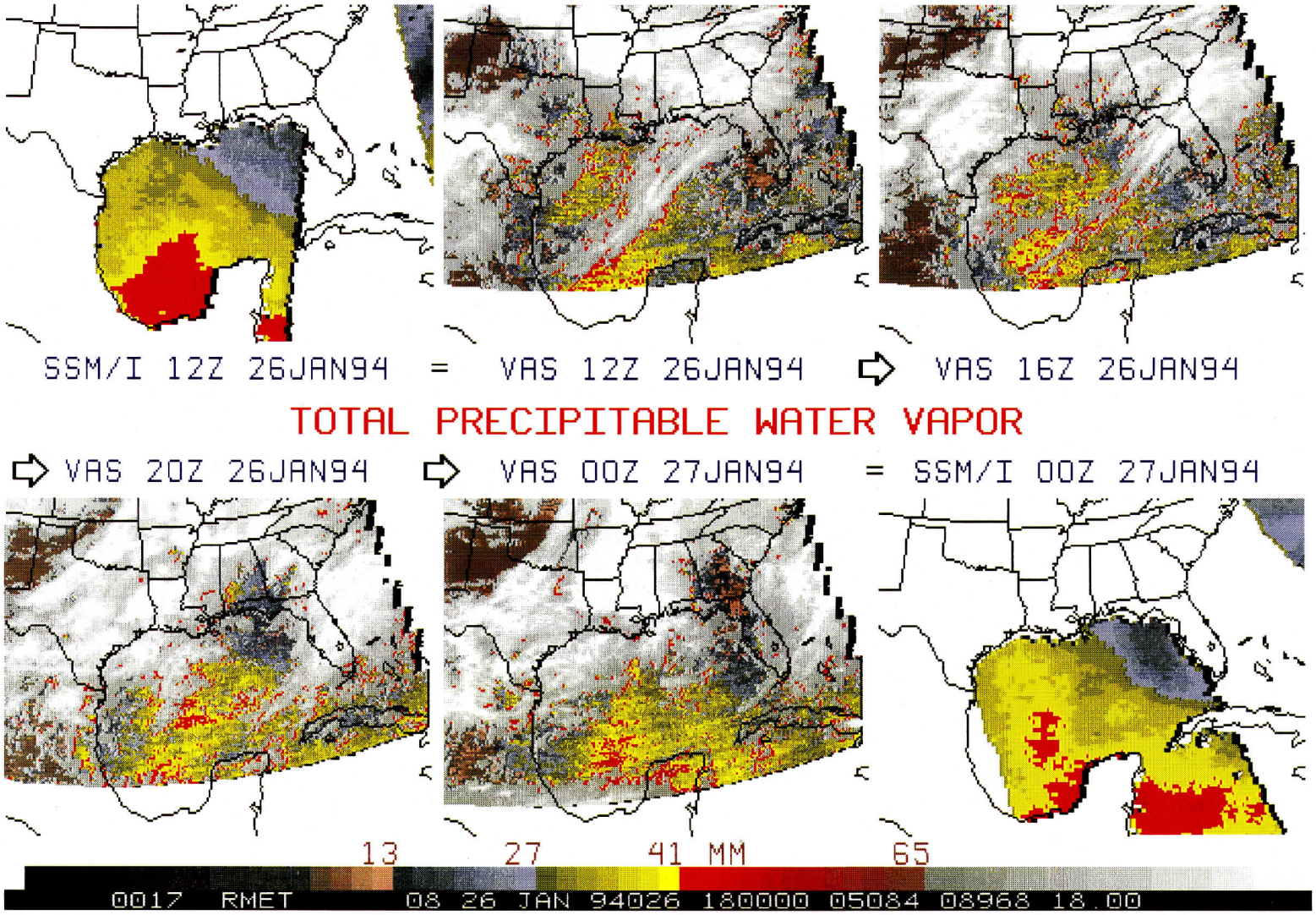
SSM/I 12Z 26JAN94 = VAS 12Z 26JAN94 ⇨ VAS 16Z 26JAN94
TOTAL PRECIPITABLE WATER VAPOR
⇨ VAS 20Z 26JAN94 ⇨ VAS 00Z 27JAN94 = SSM/I 00Z 27JAN94
13 27 41 MM 65
0017 RMET 08 26 JAN 94026 180000 05084 08968 18.00

F. Characteristics of Return Flow Events from the Gulf of Mexico - A Forecasting Perspective. Contributed by Robert M. Rabin and Gary S. Wade.

The purposes of this ongoing study are to (1) expand our understanding of the evolution of return flow to the U.S. following intrusions of cold, dry air over the Gulf of Mexico, (2) identify problems in forecasting return of atmospheric moisture to the U.S., and (3) explore the utility of satellite observations in determining the conditions leading to moisture return.

Characteristics of return flow events and forecast errors were determined from a survey of on-duty forecasters during 3 winter seasons (November to March, 1989-1992). In addition, individual events were examined in more detail using operational model output, and rawinsonde and satellite observations.

The duration and intensity of cold air intrusions and return flow in this study were similar to those found in previous studies (Crisp and Lewis, 1992). This research is unique in that it considered the vertical depth of moisture from rawinsonde and satellite. For example, the depth of moisture along the U.S. Gulf coast generally increases to 1.5-2.0 km within 24 hours of start of onshore winds. The prevailing upper air pattern was either zonal or a trough was located to the west of Texas during return flow. In addition, sea fog developed in about a third of the return flow events.

The NGM and AVN models were superior to the LFM in forecasting the development of return flow. Corroborating previous findings (Janish and Lyons, 1992), the NGM underestimated the rate of moisture during the initial phase of return flow (Figure 1).

The total precipitable water (PW) derived from the Special Sensor Microwave Imager (SSM/I) aboard the Defense Mapping Satellites was related to the depth of atmospheric moisture, as measured by coastal rawinsondes along the Texas coast (Figure 2). The results indicate that the SSM/I PW observations should be useful in identifying the moisture depth during return flow situations in the western Gulf to within 50-100 hPa. Identification of deep moisture bands over the Gulf has potential applications in forecasting heavy precipitation where upper air data is sparse. Also, the fields of PW would help the forecaster determine if numerical guidance was on the right track during its forecast of moisture return from the Gulf.

List of Figures

1. Comparison of PW from SSM/I and 48-h NGM forecast for off the upper Texas coast near 28 N, 95 W (Feb. 15-18, 1991).

2. Depth of moisture versus PW determined from SSM/I .

Figure 1

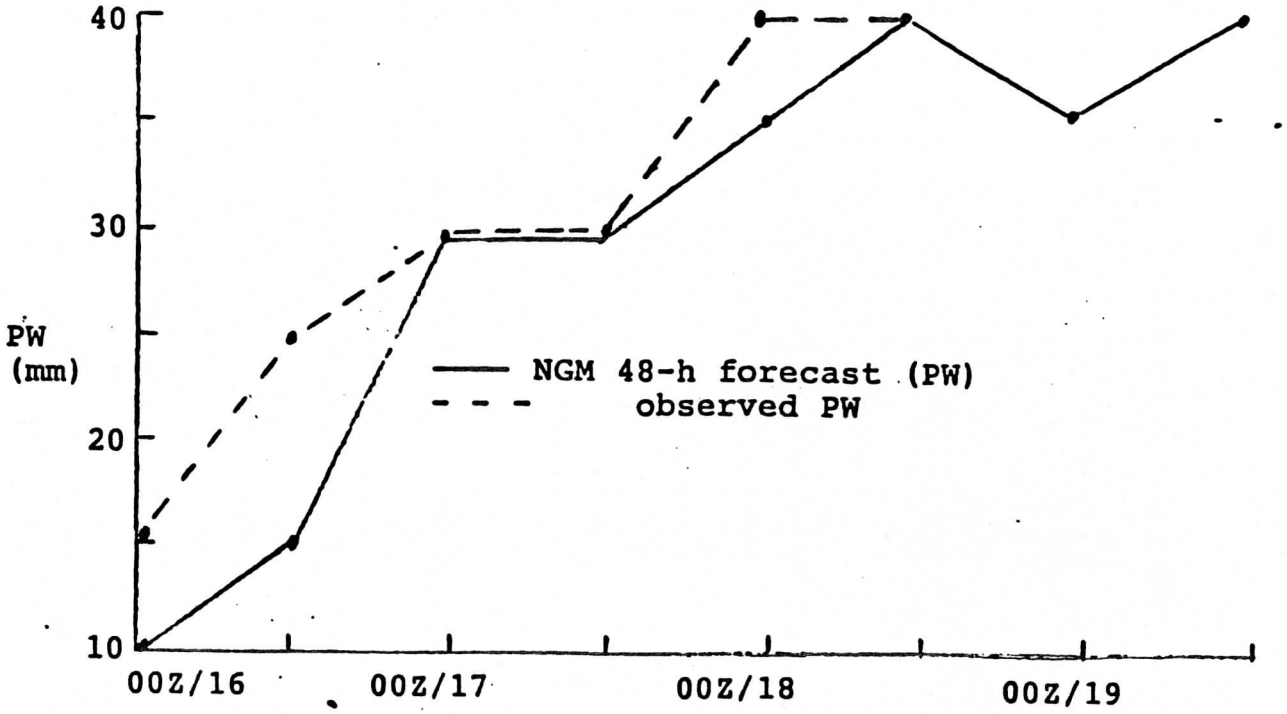

Figure 2

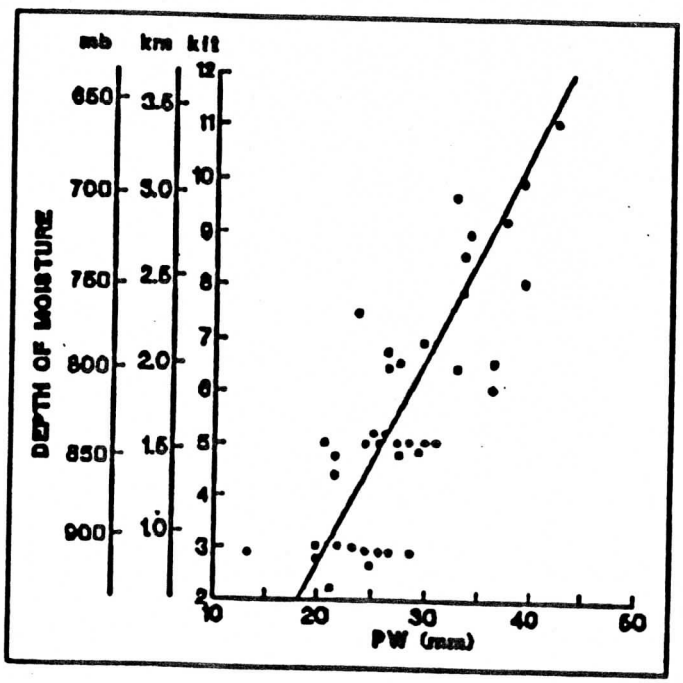

G. Multi-angle Sea Surface Temperature (MASST). Contributed by Xiangqian Wu.

Introduction

A current technique to retrieve sea surface temperature (SST) from Advanced Very High Resolution Radiometer (AVHRR) developed by McClain et al., (1985) relies on differential absorption of water vapor in a number of (window) channels, thus the name multi-channel sea surface temperature (MCSST). This technique is potentially vulnerable to volcanic aerosol contamination, whose 4-dimensional distribution and optical properties are less known than water vapor. A method to correct for this contamination would be to view the same area from various angles over a period of time, where each angle represents a particular path length. If sufficient data are collected to perform a regression of the apparent SST on path length, it is possible to extrapolate to zero path length, thus effectively removing all absorption. Such a tchnique can be attempted using AVHRR observations from different NOAA satellites.

Data

AVHRR data collected during Tropical Ocean Global Atmosphere (TOGA) Coupled Ocean-Atmosphere Response Experiment (COARE) was used for this experiment. Mr. Wick of Colorado Center for Astrodynamics Research, University of Colorado provided calibration and navigation software.

Early Results and Summary

Some preliminary results of this project are shown in Figure 1. A scatter diagram of apparent SST vs. sec(θ) is shown, where θ is local zenith angle of satellite. It is based on 20 passes, by 2 satellites (NOAA-11 & NOAA-12), at one km. (LAC) resolution, over a 10 day period, and covers a 5-by-5 lat./lon. square centered at (2.5N, 157.5E). Clouds were screened by a spatial coherence method (Coakley and Bretherton, 1982) in a box of 4-by-4 pixels. Averages of boxes whose standard deviation is greater than 0.2K (2 sigma of instrument noise) or the average itself, if less than 280 K, are thought cloud contaminated and have been excluded from the SST-sec(θ) plot. In order to remove most of the outliers, those averages that passed the cloud clearing are then divided into categories of 0.01 of sec(θ) and only the medians from each category are plotted in Figure 1. Although encouraging, Figure 1 does display some unexplained problems. For example, the SST at sec(θ)=0 is only 300.4 K, somewhat lower than the expected value of 302 K.

Figure 1

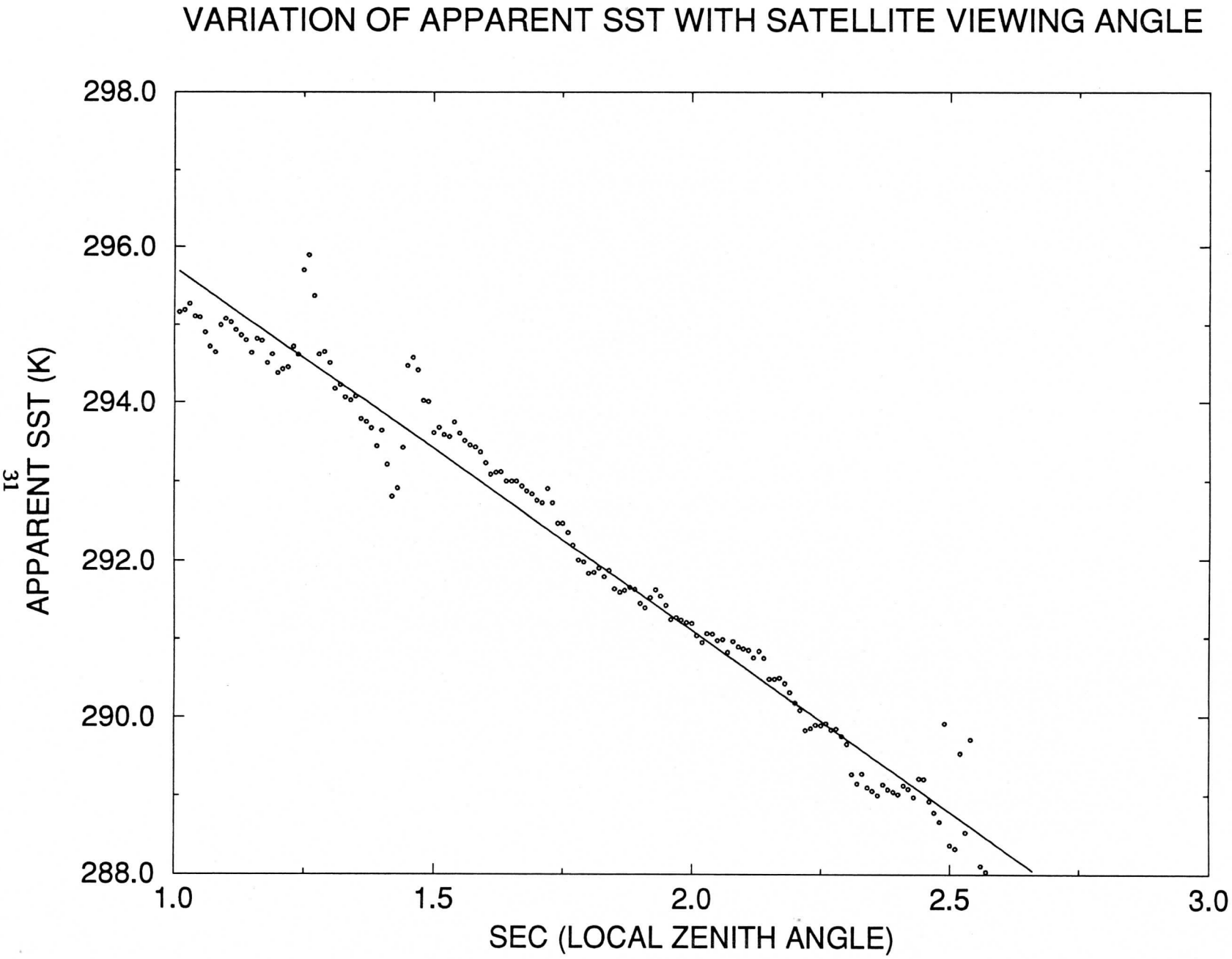
VARIATION OF APPARENT SST WITH SATELLITE VIEWING ANGLE
298.0
296.0
294.0
292.0
290.0
288.0
APPARENT SST (K)
1.0
1.5
2.0
2.5
3.0
SEC (LOCAL ZENITH ANGLE)

H. The Retrieval of Sea Surface Skin Temperature Utilizing Radiance Measurements Taken from the High Spectral Resolution Interferometer Sounder. Contributed by Nicholas R. Nalli.

HYPOTHESIS

Resolving power limitations in current infrared (IR) satellite radiometers constrain the accuracy of retrieving global sea surface temperature (SST) to about 1 K. However, the required accuracy necessary for climate studies is 0.3 K. Problems inherent in the multi-channel algorithms include the assumption that $\varepsilon=1$ (blackbody sea surface), and the necessity of empirical coefficients derived from buoy measured bulk surface temperature which differs from the actual radiometric skin temperature. A solution to these problems is now possible by using high spectral resolution radiance observations in micro-window regions taken by the High resolution Interferometer Sounder (HIS). The theoretical basis for a HIS SS Skin T (SSST) retrieval is summarized here.

The Radiative Transfer Equation (RTE) for up welling monochromatic radiance R (m.W./m/ster./cm^{-1}) at wave number, ν (cm^{-1}), at the top of the atmosphere (TOA) is given by:

$$\underset{1}{R_\upsilon} = \underset{2}{\varepsilon_\upsilon \cdot B_\upsilon(T_{skin}) \cdot \tau_\upsilon} + \underset{3}{r_\upsilon \cdot A_\upsilon^{\downarrow} \cdot \tau_\upsilon} + \underset{4}{A_\upsilon^{\uparrow}} \qquad [1]$$

where 1 is the radiance at the TOA, 2 is the surface skin emission, 3 is the surface reflection of atmospheric emission and 4 is the atmospheric emission. We here realize that $\varepsilon_\nu < 1$, thus the reflection term cannot be ignored. The reflected energy of the small down welling atmospheric emission off absorption lines by the ocean might be accounted for by introducing an "effective emissivity" ε_ν^* of the ocean's surface such that

$$\varepsilon_\upsilon^* = \frac{\varepsilon_\upsilon \cdot B_\upsilon(T_{skin}) + r_\upsilon \cdot A_\upsilon^{\downarrow}}{B_\upsilon(T_{skin})} = \varepsilon_\upsilon + \frac{r_\upsilon \cdot A_\upsilon^{\downarrow}}{B_\upsilon(T_{skin})} \qquad [2]$$

It thus follows from [1] that

$$\underset{1}{R_\upsilon} = \underset{2}{\varepsilon_\upsilon^* \cdot B_\upsilon(T_{skin}) \cdot \tau_\upsilon} + \underset{4}{A_\upsilon^{\uparrow}} \qquad [3]$$

B (T_{skin}) can be approximated by the first order Taylor series polynomial:

$$B_\upsilon(T_{skin}) = B_\upsilon(T_o) + (T_{skin} - T_o) \cdot \left.\frac{\partial B_\upsilon(T)}{\partial T}\right|_{T_o} \qquad [4]$$

where T_0 is the highest off-line T_B in the observed spectrum.

Plugging [4] into [3], and assuming that ε^* is constant with wave number yields

$$\frac{R_\upsilon - A_\upsilon^{\uparrow}}{\tau_\upsilon \cdot B_o} = \varepsilon^* + \varepsilon^* \cdot (T_{skin} - T_o) \cdot \left(\frac{1}{B_\upsilon(T_o)}\right) \cdot \left(\left.\frac{\partial B_\upsilon(T)}{\partial T}\right|_{T_o}\right) \qquad [5]$$

Given n spectral off-line HIS radiance R_ν measurements, and atmospheric profiles of temperature and water vapor, it is possible to solve the n linear equations represented by [5] for the two unknowns ε^* and T_{skin} using a least-squares regression technique. Since this retrieval method retains most of the RTE with minimal assumptions it is anticipated that a more accurate determination of the sea surface skin temperature is possible.

ANALYSIS

The validation of the proposed algorithm has thus far concentrated on simulated data derived from FASCOD3, a sophisticated radiative transfer model. The initial results using noise-free data over a narrow spectral range (900-1100 cm^{-1}) look promising (Figure 1). However, the addition of instrument noise is sure to contaminate the results. Therefore, consideration has been given to using a broader spectral range in all 3 HIS bands to reduce the effects of noise by obtaining more measurements. Unfortunately, the broader the spectrum, the less valid is our assumption of a spectrally constant ε^*. By incorporating a spectrally varying $\varepsilon_\nu{}^*$ we note that [5] now becomes a system of n equations with n + 1 unknowns; thus, a further constraint is necessary. This is the focus of present research. When a known $\varepsilon_\nu{}^*$ spectrum is used, the algorithm appears to work well in the presence of random noise (Figure 2).

The goal of future research is the testing of the algorithm against real, co-added HIS aircraft data taken over oceanographic drifting buoys during the Convection and Atmospheric Moisture EXperiment (CAMEX). The buoy measured bulk surface temperature would provide an approximate ground truth for comparison.

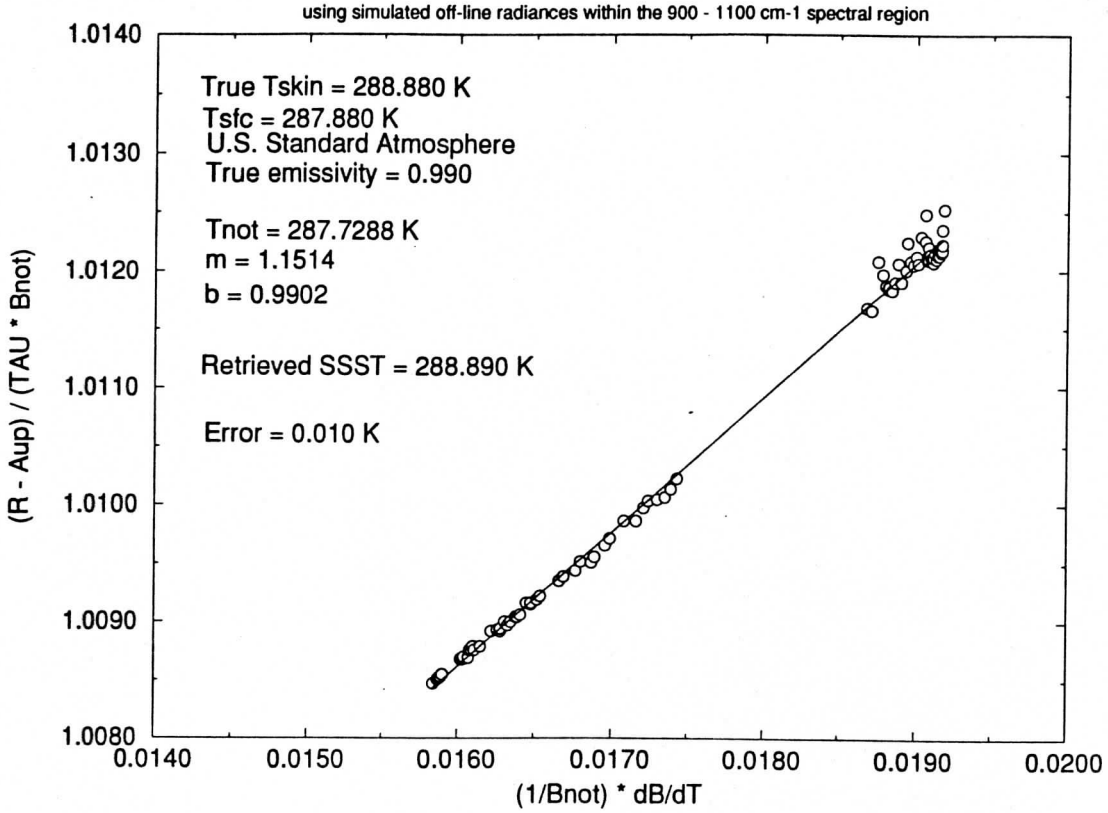

Figure 1
HIS SSST retrieval from noise-free data and constant ε^* assumption.

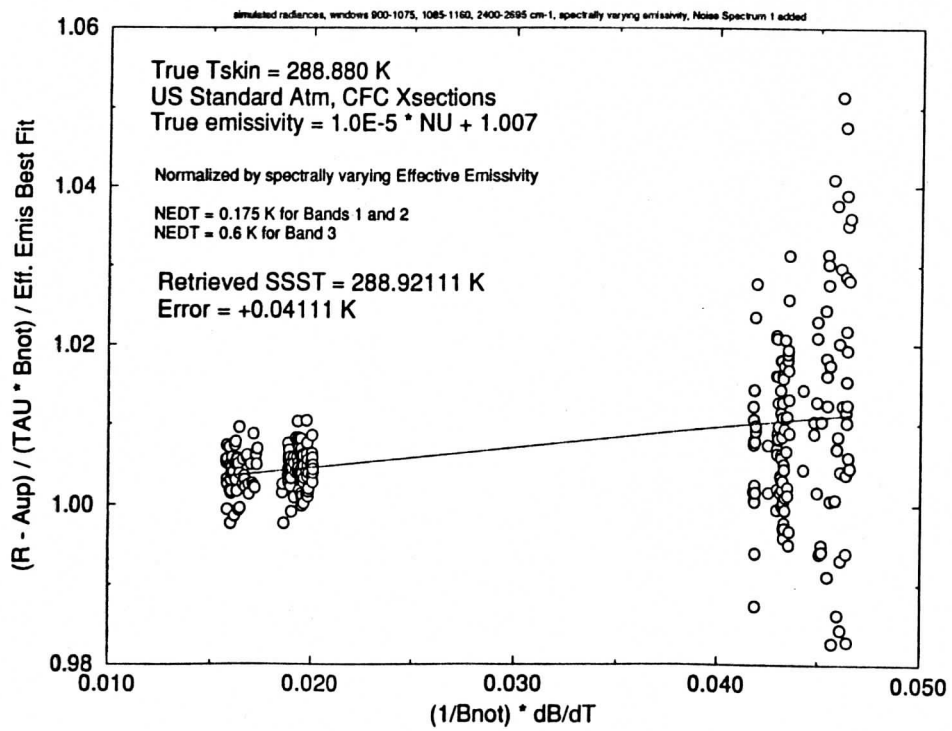

Figure 2
HIS SSST retrieval from noisy data and a known ε_{υ}^* spectrum.

I. The Use of the Downward and Upward High resolution Interferometer Sounder (HIS) for the Convection and Atmospheric Moisture EXperiment (CAMEX). Contributed by William L. Smith and Robert O. Knuteson.

Introduction

A multi-purpose field experiment was conducted between 10-30 September 1993 at Wallops Island. The objectives of the experiment were fourfold. First to validate water substance emitted radiances measured by the Defense Meteorological Satellite Program (DMSP) Satellite Sensor Microwave/Temperature-2 (SSM/T-2) sensor. Second, to determine experimentally the water vapor profile capability of current satellite, future satellite, and ground-based active and passive systems. Third, to provide time and space coincident measurements of atmospheric temperature and water vapor profiles and up welling and down welling infrared spectral radiance measurements as needed for validation purposes. Finally, to measure the radiative and micro physical properties of precipitation using a combination of active and passive microwave radars and radiometers aboard the ER-2 aircraft, and on the ground, and to relate these measurements to those from passive microwave radiometers aboard the DMSP satellite. The goal of the University of Wisconsin was to demonstrate the atmospheric and surface sensing capabilities of the HIS aboard the NASA ER-2 aircraft and the Ground-Based HIS (GB-HIS). The purpose of this report is to provide a brief summary of the data acquisition and an overview of some of the early results.

Background and Data

The atmospheric radiance contained within this data set was observed using the HIS, a Fourier transform spectrometer developed at the University of Wisconsin for remote sensing of the atmosphere and earth at high spectral resolution and with high absolute accuracy. The instrument is a Michelson interferometer with laser sampling for wave number accuracy and onboard precision blackbodies for radiometric accuracy. The HIS has been operated both from aircraft looking down at the atmosphere and the earth's surface and from the surface looking upward to measure the up welling and down welling atmospheric radiance, respectively. The HIS data consists of atmospheric radiance divided into three broad bands spanning the infrared spectrum from 3.7 to 16.7 μm at a spectral resolution of between 0.3 and 1.0 cm^{-1} depending on spectral band. The instrument field of view is approximately 2 km. at 20 km range.

The data set described here is derived from flights aboard the NASA high altitude U2/ER-2 research aircraft which flew in the stratosphere at about 20 km altitude during the CAMEX based at Wallops Island. A complete list of flights of the HIS during CAMEX is given in Table 1.

Table 1. HIS CAMEX DATA ACQUISITION SUMMARY

Flight No.	ER-2 Mission	DATE	TIME (UTC)	COMMENTS
93-164	Ferry Flight (CA-VA)	12 Sep. 1993	20:11-02:27	Variety of Scenes.
93-165	1st DMSP Overpass	15 Sep. 1993	20:23-20:45	Aborted, ER-2 Failure.
93-166	Ocean Convection	19 Sep. 1993	20:22-20:56	Aborted, ER-2 Failure.
93-167	ER-2 Checkout Flight	25 Sep. 1993	16:25-17:55	
93-168	Ocean Convection	26 Sep. 1993	19:15-22:55	
93-169	AIRS Flight	29 Sep. 1993	01:20-04:39	Good Ground Truth.
93-178	2nd DMSP Overpass	30 Sep. 1993	20:21-01:40	
94-001	Ocean Convection-Florida	03 Oct. 1993	20:15-02:50	
94-002	Ocean Convection-Florida	05 Oct. 1993	16:13-22:59	

The UW CAMEX data set is comprised of three parts; time sequence data, validation data, and auxiliary data. The time sequence data includes the time sequence of radiance spectra from the HIS instrument, the ER-2 navigation and in-situ sampling data, and the balloon sonde ascent data. The time sequence data is most appropriate for characterization of variations in the atmospheric state in both time and space. The validation data consists of a low noise HIS spectrum of up welling radiance and a file containing a best estimate of the atmospheric state parameters consistent with the time and place of the HIS observation. This atmospheric state profile is derived from coincident temperature, moisture, and ozone sondes. The validation data is most valuable for use in detailed comparison with line-by-line radiative transfer calculation model calculations. The auxiliary data includes all other measurements relevant to the characterization of the earth-atmosphere system at the time of the HIS measurements. In particular, these include the other ER-2 instruments, e.g. microwave sensors, the RAMAN water vapor profiles from Wallops Island, visible and IR satellite images, surface land and ocean buoy observations, and profiles from the AERI ground based infrared system. These auxiliary data are either from the UW or directly from the appropriate Principle Investigators' instruments. This data set includes data from the 12 September 1993 ferry flight and the 29 September 1993 AIRS flight.

Early Results

For the 29 September 1993 case Figure 1 shows a comparison of radiant brightness temperature observed with the HIS and that calculated on the basis of simultaneous rawinsondes using the latest line by line spectroscopic radiative transfer model, FASCOD-3P. Significant differences between the observed and calculated brightness temperature spectra are not due to observation error (believed to be less than 0.5°K) but rather due to errors in the rawinsonde estimate of the atmospheric state and to errors in the line parameters used to calculate the up welling radiance. In fact spectroscopists are interested in using comparisons like that shown in Figure 1 in order to resolve uncertainties in absorption line parameters, particularly line shape approximations, which are difficult to verify without experimental radiance data as presented in Figure 1.

Figure 2 shows a comparison between a rawinsonde (weather balloon) atmospheric temperature and dew point temperature observation and a sounding retrieved from the HIS radiance spectrum observed over Wallops Island at the time of the rawinsonde launch. Also shown for comparison is the "retrieval" from the TIROS Operational Vertical Sounder (TOVS) aboard the NOAA satellite orbiting over Wallops Island near the time of the rawinsonde launch. These comparisons provide experimental confirmation of the dramatic improvements expected from theory in the vertical resolution and accuracy of the atmospheric profiles retrieved using higher spectral resolution radiance observations.

Summary

The UW CAMEX data set is a collection of atmospheric state profiles and coincident up welling radiance observations at 20 km altitude from the HIS. These data are available from the University of Wisconsin for use with modes of radiative transfer and for remote sensing studies of the atmosphere and land surface. Early results show the advantages of remote sensing the atmosphere and surface with high spectral resolution radiance measurements. The data from these instruments should greatly advance our knowledge of earth-atmosphere composition and the physical processes important for environmental monitoring and prediction.

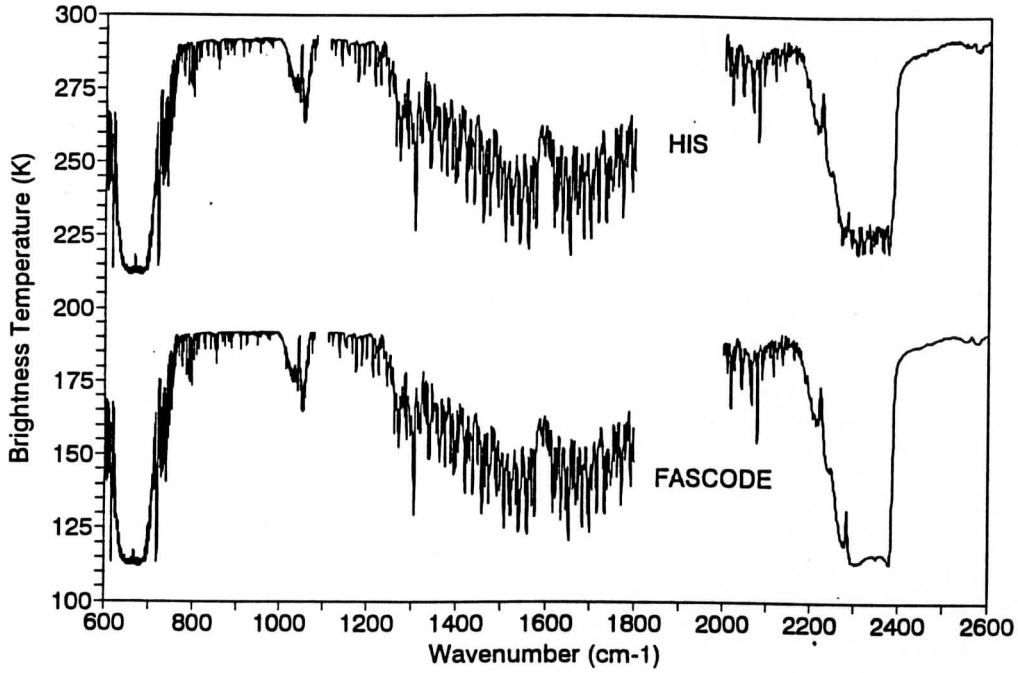

Figure 1: Comparison between an observed and calculated brightness temperature spectrum for 29 September, 1993 at Wallops Island, VA.

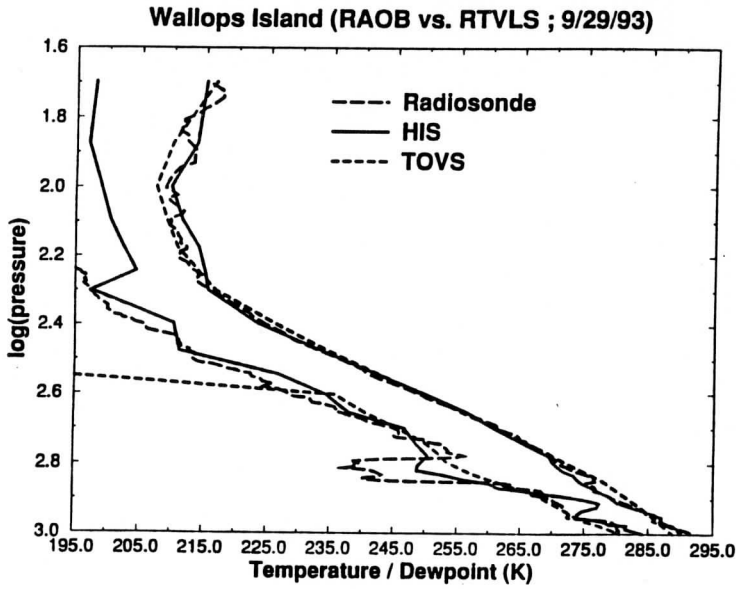

Figure 2: Comparison between a Radisonde observation and Radiometrically Retrieved Atmospheric Soundings for High (HIS) and Low (TOVS) spectral Resolution Instruments.

J. A Comparison of POES Satellite Derived Wind Techniques in the Arctic at CIMSS.

Contributed by Leroy D. Herman and Frederick W. Nagle

Two techniques for obtaining vectors from Polar Orbiting Environmental Satellite (POES) observations are examined. These are: (1) Cloud tracking with infrared imagery and CO_2 altitude assignment, and (2) Cluster fitting of gradients from temperature retrievals to obtain gradient winds. Each of these methods has features that make it desirable. The first of these, cloud tracking with infrared, is relatively fast and permits operator intervention in the selection of tracking targets or the deletion of vectors. The second technique, cluster fit of gradients, provides an approach which allows the determination of winds at any level in the atmosphere using an inference of gradients from retrievals.

The cluster technique uses a cluster of neighboring temperature retrievals, typically 40 in number, to infer the pressure height field at 10 levels by fitting a cubic surface. Two spatial derivatives of this surface provide estimates of the wind and its deformation. Goodness of the RMS fit and values of deformation are criteria used in judging the accuracy of the winds. This method works best with minimum cloud conditions.

The improvements obtained with the CO_2 slicing method indicate it produces more accurate altitudes than the original infrared altitude assignment. Both it and the cluster fit technique provide high quality data, and, when used together, greater coverage. Results indicating significant improvements in satellite winds are possible using this combination of techniques.

TABLE 1. Comparison of the mean vector difference between rawinsondes and three techniques of obtaining vectors.

	POES		**CO2**		**GRADIENT**	
Day	Num	Avg	Num	Avg	Num	Avg
1	17	5.39	26	4.51	24	9.09
2	21	7.22	19	5.40	369	10.2

Table 1 is a comparison between the errors obtained from the three methods with rawinsonde vectors. It shows how CO_2 winds are better than either the POES and gradient winds. In addition the POES winds are better than the gradient winds. These two cases were made during the fall of 1993 when there was a mixture of clear and cloudy areas in the Arctic. The gradient technique then used a method of fitting a cluster 24 points in determining the gradient.

As a result of experimenting with the gradient technique in a variety of cases, it was found that an improvement occurs when the fit was made to 40 points instead of 24. In this case the improvement in gradient winds is shown in Table 2. These were made during the winter when the cold Arctic

atmosphere has few clouds to track, so no meaningful observations could be gathered by the POES and CO2 method.

TABLE 2. Gradient wind results by comparing with rawinsondes.

	GRADIENT	
Day	Num	Avg
3	146	5.49
4	432	8.34
5	641	6.17

III. PERSONNEL AND EQUIPMENT

Personnel

	LABOR (%)	COMPUTER (%)
SSEC		
Anthony J. Schreiner	20	30
William H. Raymond	75	0
Robert O. Knuteson	10	0
William L. Smith	10	0
Xiangqian Wu	100	100
Xiaohua Wu	100	100
Nicholas R. Nalli	30	
NESDIS		
Christopher M. Hayden		40
Gary S. Wade		60
Robert M. Aune		85
Leroy D. Herman		90
Geary M. Callan		40
Robert M. Rabin		10
Frederick W. Nagle		10
Visiting Scientist	0	0

The numbers underneath the column "LABOR" represent the percentage of their labor time which was charged to this project. The percentages below the column headed by "COMPUTER" indicate the amount of computer time which the scientists charged to this contract. Both percentages are based on one year being equivalent t 100%. NESDIS employees' labor is provided from funds outside of this contract.

Equipment

None

IV. SUMMARY

The support from this contract has been important in providing the programmers, research scientists, and support staff the opportunity to perform a wide variety of research within the CIMSS organization. Many of the areas of research which were discussed in Section III are ongoing topics.

V. REFERENCES

Chesters, D., L.W. Uccellini, and W.D. Robinson, 1983: Low-Level water vapor fields from the VISSR Atmospheric Sounder (VAS) "split window" channels. *J. Clim. Appl. Meteor.*, **22**, 725-743.

Coakley, J. A., and F. P. Bretherton, 1982: Cloud cover from high-resolution scanner data: Detecting and allowing for partially filled fields of view. *J. Geophys. Res.*, **87**, (C7) 4917-4,932

Crisp, C.A., J.M. Lewis, 1992: Return flow in the Gulf of Mexico. Part I: A Classificatory approach with a global historical perspective. *J. Appl. Meteor.*, **31**, 868-881.

Eyre, J. R., 1991: A new fast radiative transfer model for TOVS. *Technical Proceedings, Sixth International TOVS Study Conference*, May 1-6, 1991, Airlie, VA.. CIMSS, 1225 W. Dayton St.., Madison, WI. 118-133.

Fuelberg, H.E. and P.J. Meyer, 1986: An analysis of mesoscale VAS retrievals using statistical structure functions. *J. Clim. Appl. Meteor.*, **25**, 59-76.

Hayden, C.M., 1988: GOES-VAS simultaneous temperature-moisture retrieval algorithm. *J. Appl. Meteor.*, **27**, 705-733.

Hayden, C. M. and T. J. Schmit, 1991; The anticipated sounding capabilities of GOES-I and beyond. *Bull. Amer. Meteor. Soc.*, **72**, 1835-1846

Hayden, C. M., and X. Wu, 1994: Upper tropospheric relative humidity estimates from GOES. *8th Conf. Atmos. Rad.*, pp.58-60. 23-28 January 1994, Nashville, TN. Amer. Meteor. Soc., Boston, MA

Herman, Leroy D., 1993: High frequency satellite cloud motion at high latitudes. *8th Symposium on Meteorological Observations and Instrumentation*, 17-22 January 1993, Anaheim CA. Amer. Meteor. Soc., Boston, MA. pp.465-468.

Janish, P., and S. W. Lyons, 1992: NGM performance during cold-air outbreaks and periods of return flow over the Gulf of Mexico with emphasis on moisture-field evolution. *J. Appl. Meteor.*, **31**, 995-1017.

Johnson, G. Alan and R.M. Rabin, 1993: Highlights of return flow events from the Gulf of Mexico during 1989-1992 winters - a forecasting perspective. *13th Conference on Weather Forecasting and Analysis*, 1-6 August 1993, Vienna, VA. Amer. Metior. Soc., Boston, MA.

McClain, E. P., W. G. Pichel, and C. C. Walton, 1985: Comparative performance of AVHRR-based multi-channel sea surface temperatures. *J. Geophys. Res.*, **90**, 11587-11601

Moller, F., 1961: Atmospheric water vapor measurements at 6-7 microns from a satellite. *Planet. Space Sci.*, **5**, 202-206

Orlanski, I., 1981: The quasi-hydrostatic approximation. *J. Atmos. Sci.*, **38**, 572-582.

Perkey, D.J., 1976: A description of preliminary results from a fine-mesh model for forecasting quantitative precipitation. Mon. Wea. Rev., 104, 1209-1235.

Raschke, E. and W. R. Bandeen, 1967: A quasi-global analysis of tropospheric water vapor content from TIROS-IV radiation data. *J. Appl. Meteor.*, **6**, 468-481.

Schmetz, J., and O. M. Turpeinen, 1988: Estimation of the upper tropospheric relative humidity field from METEOSAT water vapor image data. *J. Appl. Meteor.*, **27**, 889-899

Smith, W.L., V.E. Suomi, W.P. Menzel, H.M. Woolf, L.A. Sromovsky, H.E. Revercomb, C.M. Hayden, D.N. Erickson, and F.R. Mosher, 1981: First sounding results from VAS-D. *Bull. Amer. Meteor. Soc.*, **62**, 232-236.

Smith, W.L., H.M. Woolf, and A.J. Schreiner, 1985: Simultaneous retrieval of surface atmospheric parameters: a physical and analytically direct approach. *Advances in Remote Sensing*. A. Deepak, H.E. Fleming, and M.T. Chahine (Eds.), A. Deepak Pub. ISBN 0-937194-07-7, 221-232.

Soden, B. J., and F. P. Bretherton, 1993: Upper tropospheric relative humidity from the GOES 6.7 mm channel: Method and climatology for July 1987. *J. Geophys. Res.*, **98**, 16669-16688

Soden, B. J., S. A. Ackerman, R Ferrare. and D. O'C Starr, 1994: Comparison of upper tropospheric water vapor from GOES, Raman Lidar, and CLASS measurements during FIRE Cirrus-II. Submitted to: *J. Geo. Res.*

Starr, D. O'C., and S. H. Melfi, 1991: The role of water vapor in climate: a strategic research plan for the proposed GEWEX water vapor project (GVaP). *NASA Conf. Publication*, 3120, 50 pp.

Susskind, J., J. Rosenfield, D. Reuter, and M.T. Chahine, 1984: Remote sensing of weather and climate parameters for HIRS2/MSU on TIROS-N. *J. Geophys. Res.*, **89**, 4677-4697.

Xiaohua Wu, 1993: Short-range precipitation forecasts using assimilation of simulated satellite water vapor profiles and cloud liquid water. Ph.D dissertation, University of Wisconsin - Madison. 182pp.

Wu, X., J. J. Bates, and S. J. S. Khalsa, 1993: A climatology of water vapor band brightness temperatures from NOAA operational satellites. *J. of Clim.* **6**, 1282-1300.